Atomic Layer Deposition of TaN, NbN, and MoN Films for Cu Metallizations

Petra Alén

Laboratory of Inorganic Chemistry
Department of Chemistry
University of Helsinki
Finland

ACADEMIC DISSERTATION

To be presented with the permission of the Faculty of Science of the University of Helsinki for public criticism in Auditorium A129 of the Department of Chemistry, A. I. Virtasen aukio, on June 22nd, 2005 at 12 o´clock noon.

Helsinki 2005

ISBN 952-91-8796-3 (Paperback)
ISBN 952-10-2497-6 (PDF)
http://ethesis.helsinki.fi
Yliopistopaino
Helsinki 2005

Supervisors

Prof. Mikko Ritala
and
Prof. Markku Leskelä
Laboratory of Inorganic Chemistry
Department of Chemistry
University of Helsinki
Finland

Reviewers

Prof. Charles H. Winter
Department of Chemistry
Wayne State University
United States

Prof. Tapio Mäntylä
Institute of Materials Science
Tampere University of Technology
Finland

Opponent

Dos. Jyrki Molarius
Information Technology
VTT Technical Research Centre
Finland

Abstract

Transition metal nitrides, metal silicides, and metal-silicon-nitrides are considered the most promising diffusion barrier materials for next generation ultra large scale integration (ULSI) microelectronics. The semiconductor industry has long used Ti, Ta, and W based materials, and their material properties have been very well studied. Recently, tantalum-based materials have been attracting particular interest. The barrier properties of materials based on other transition metals have been little studied. In this work, tantalum nitride films were deposited, with four new reducing agents used to reduce tantalum and obtain the desired TaN phase. As well, the deposition of niobium and molybdenum nitride films was investigated. All films were deposited by the atomic layer deposition (ALD) method, which ensures excellent conformality and large area uniformity of the films.

The problem in depositing TaN films by ALD is that in volatile tantalum precursors the tantalum usually exists in oxidation state +V which is difficult to reduce to the +III state needed in cubic TaN. The new reducing agents examined in this study were trimethylaluminum (TMA), *tert*-butylamine ($^{t}BuNH_2$), allylamine (allylNH_2), and tris(dimethylamino)silane (TDMAS). In addition to reducing tantalum, TMA also acted as a carbon and aluminum source, $^{t}BuNH_2$ and allylNH_2 as nitrogen sources, and TDMAS as a silicon precursor.

ALD of niobium nitride and molybdenum nitride films was studied at lower temperatures than reported earlier. Both NbN_x and MoN_x films were deposited from the corresponding metal chloride precursors ($NbCl_5$ and $MoCl_5$, respectively) using ammonia as nitrogen source. No additional reducing agent was required.

The deposition parameters, compositions, crystallinity, and electrical properties were studied for all deposited films. Barrier characteristics were investigated for Ta(Al)N(C), NbN_x, and MoN_x films. The work function values were measured for Ta(Si)N films deposited at two different temperatures.

Preface

This thesis is based on the experimental work done during the years 1999 – 2005 in the Laboratory of Inorganic Chemistry at the University of Helsinki.

I am most grateful to my supervisors Professor Mikko Ritala and Professor Markku Leskelä for their excellent guidance during this work.

I wish to thank my co-workers, especially Dr. Marika Juppo, for her advices and support. I am also grateful to Dr. Timo Sajavaara and Dr. Kai Arstila for the TOF-ERD analysis of the films. The assistance of Kathleen Ahonen for revising the language of this thesis is gratefully acknowledged.

I want to thank my roommates Dr. Marika Juppo and Mr. Marko Vehkamäki and all the staff in the Laboratory of Inorganic Chemistry for the pleasant and inspiring working atmosphere. The interesting coffee break discussions have really cheered up the working days.

Finally, warmest thanks go to my parents Ritva and Heikki for their continuous support and belief in me. Above all, I would like to thank my husband Juha and our son Niklas for all your love.

Special thanks go to Master and Quincy for the enjoyable moments.

Financial support from the Academy of Finland, the Finnish National Technology Agency (TEKES), Nokia Foundation, Association of Finnish Chemical Societes, and Acta Chemica Scandinavica is gratefully acknowledged.

Helsinki, June 2005

Petra Alén

List of publications

This work is based on the following publications, which are referred in the text by their Roman numerals:

I P. Alén, M. Juppo, M. Ritala, T. Sajavaara, J. Keinonen, and M. Leskelä: Atomic Layer Deposition of Ta(Al)N(C) Thin Films Using Trimethylaluminum as a Reducing Agent, *J. Electrochem. Soc.* 148 (2001) G566-G571.

II P. Alén, M. Juppo, M. Ritala, M. Leskelä, T. Sajavaara, and J. Keinonen: *tert*-Butylamine and Allylamine as Reductive Nitrogen Sources in Atomic Layer Deposition of TaN Thin Films, *J. Mater. Res.* 17 (2002) 107-114.

III P. Alén, M. Juppo, M. Ritala, M. Leskelä, T. Sajavaara, J. Keinonen, J.C. Hooker, and J.W. Maes: ALD of Ta(Si)N Thin Films Using TDMAS as a Reducing Agent and as a Si Precursor, *J. Electrochem. Soc.* 151 (2004) G523-G527.

IV P. Alén, M. Ritala, K. Arstila, J. Keinonen, and M. Leskelä: The Growth and Diffusion Barrier Properties of Atomic Layer Deposited NbN_x Thin Films, *Thin Solid Films*, in press.

V P. Alén, M. Ritala, K. Arstila, J. Keinonen, and M. Leskelä: Atomic Layer Deposition of Molybdenum Nitride Thin Films for Cu Metallizations, *J. Electrochem. Soc.* 152 (2005) G361-G366.

Contents

List of abbreviations and acronyms

AES	Auger electron spectroscopy
ALD	Atomic layer deposition
allylNH_2	Allylamine
CMOS	Complementary metal oxide semiconductor
CVD	Chemical vapor deposition
Cy	Cyclohexyl
DMHy	1,1-Dimethylhydrazine
EDX	Energy dispersive X-ray spectroscopy
EOT	Equivalent oxide thickness
FGA	Forming gas anneal
HMDS	1,1,1,3,3,3-Hexamethyldisilazane
IBAD	Ion beam assisted deposition
MEIS	Medium energy ion scattering
MOCVD	Metal-organic chemical vapor deposition
MOSFET	Metal oxide semiconductor field effect transistor
MRAM	Magnetic random access memory
NMOS	N-channel metal oxide semiconductor
NRB	Nuclear resonance broadening
PAALD	Plasma-assisted atomic layer deposition
PACVD	Plasma-assisted chemical vapor deposition
PAE-2	Poly(arylene ether)
PDEAT	Pentakis(diethylamido)tantalum
PDMAT	Pentakis(dimethylamido)tantalum
PEALD	Plasma-enhanced atomic layer deposition
PEMAT	Pentakis(ethylmethylamino)tantalum
PLD	Pulsed laser deposition
PMOS	P-channel metal oxide semiconductor
PVD	Physical vapor deposition
RBS	Rutherford backscattering spectrometry
RIE	Reactive ion etching
RTA	Rapid thermal annealing
sccm	Standard cubic centimeter per minute
SEM	Scanning electron microscopy
$^{t}BuNH_2$	*tert*-Butylamine
TBTDET	*tert*-Butylimidotris(diethylamido)tantalum

TDMAS	Tris(dimethylamino)silane
TEM	Transmission electron microscopy
TMA	Trimethylaluminum
TOF-ERDA	Time-of-flight elastic recoil detection analysis
TVS	Triangular voltage sweep
ULSI	Ultra large scale integration
V_{fb}	Flat band voltage
XPS	X-ray photoelectron spectroscopy
XRD	X-ray diffraction
XRR	X-ray reflectance

1. Introduction

The continuous downscaling of microelectronic devices over the last 30 years has been accomplished by shrinking the feature sizes.[1] It is not possible to carry on this shrinkage further with the materials in use today. New materials are needed to meet the requirements of the future. Copper and materials of low-dielectric constant have already partially replaced aluminum and silicon dioxide based interconnects, and metal gates are replacing polycrystalline silicon.[2]

The transition from aluminum- to copper-based interconnects in the next generation ultra large scale integration microelectronics is creating significant challenges for new barrier materials. Copper possesses many superior properties to aluminum–for example, lower bulk resistivity, higher melting point, and higher electromigration resistance–but it has the drawback of readily diffusing into silicon and insulators. The diffusion must be effectively prevented therefore, by inserting a barrier layer between copper and other materials. Transition metal nitrides, metal silicides, and metal-silicon-nitrides are the materials most studied for use as diffusion barriers.[3] One of the most promising and recently extensively studied barrier materials is tantalum nitride, which has high melting point and is both very hard and highly conductive. Niobium and molybdenum nitrides have been comparatively little studied, although they possess the same desirable properties as tantalum nitride. All these three nitrides are also thermodynamically very stable with respect to copper because they do not form compounds with it.

Besides barrier materials, transition metal nitrides have been investigated for use as gate metals. It is considered probable that metal gates will replace polycrystalline silicon in the future complementary metal oxide semiconductor (CMOS) devices. Decrease of the gate oxide thickness will increase the importance of the capacitance associated with the depletion layer at the interface between polycrystalline silicon gate electrode and gate dielectric. The gate metal material has to have an appropriate work function, high thermal stability, low reactivity, and low electrical resistivity. One of the most promising candidates to meet these requirements is Ta-Si-N.[4]

The main goal of the present study was to deposit transition metal nitride films by atomic layer deposition (ALD)[5-7] method. Films deposited by ALD have excellent conformality and large area uniformity in addition to accurately

controlled film thickness. Tantalum nitride films were deposited from tantalum pentachloride and ammonia with four different reducing agents. Niobium and molybdenum nitride films were deposited from the corresponding metal chlorides and ammonia with no additional reducing agent. Barrier properties were studied for the Ta(Al)N(C) films deposited with trimethylaluminum as an additional reducing agent and also for NbN_x and MoN_x films with and without TaN_x/TiN doping. Work function values were determined for the Ta(Si)N films deposited with use of tris(dimethylamino)silane as reducing agent and as silicon precursor.

As background for the study, the investigated materials and their major areas of application are briefly presented. General aspects of the ALD method will then be discussed. The literature relevant to tantalum nitride, niobium nitride, and molybdenum nitride films deposited by ALD is reviewed and selected examples of films deposited by other methods are introduced. The diffusion barrier performance and gate electrode properties of TaN and Ta-Si-N are described in some detail. After an account of the experimental details of film deposition and characterization, the results reported in the publications I-V are summarized.

2. Background

2.1. Transition metal nitride films

On the basis of structure transition metal nitrides can be described as interstitial alloys, where nitrogen atoms are located in the interstitial voids of the densely packed host lattice.[8] Usually, the structurally similar transition metal nitrides are able to form solid solutions with other transition metal nitrides. Transition metal nitrides have an impressive number of outstanding properties including extreme hardness, thermal integrity, high melting points, good chemical resistance, electrical conductivity, and metallic-like appearance. This combination of useful characteristics has led to numerous thin film applications, such as hard coatings, corrosion and abrasion resistant layers, and decorative coatings. Nevertheless, the fastest developing area of application today is microelectronics, where transition metal nitride films are studied for use as barriers between copper and silicon in ultra large scale integration (ULSI) devices. Besides diffusion barriers, transition metal nitrides and metal-silicon-nitrides are promising gate electrodes for complementary metal oxide semiconductor (CMOS) devices.

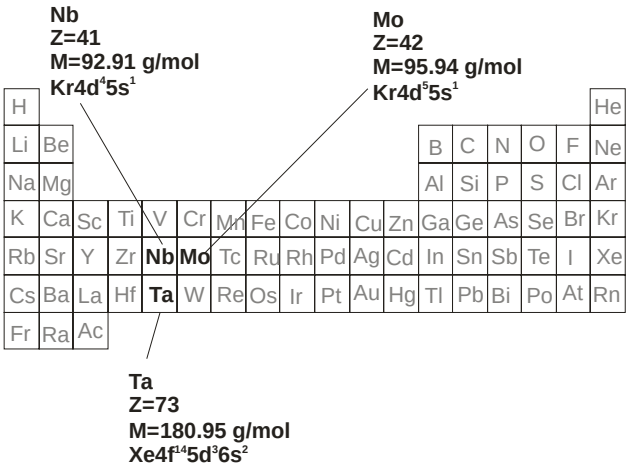

Figure 1. The materials studied in this work were tantalum nitride, niobium nitride, and molybdenum nitride.

The materials studied in this work were tantalum nitride, niobium nitride, and molybdenum nitride (Fig. 1). Since the aim of the study was to deposit nitride films (i) for barrier layers and (ii) for gate electrodes, these two applications are discussed more thoroughly in the following.

2.1.1. Tantalum nitride

Tantalum forms compounds with nitrogen in oxidation states from nearly zero up to +V (Table I).[9-11] Table I shows the Ta-N phases found in the JCPDS data base. At the highest oxidation state +V, tantalum forms a dielectric Ta_3N_5 phase. As good conductivity is required in many applications, the two conductive phases, TaN and Ta_2N, which tantalum forms in lower oxidation states have attracted most interest. Both the TaN and Ta_2N phases have high melting points and are extremely hard.[12,13]

Table I. Crystal structures and corresponding JCPDS data cards for Ta-N phases.

Ta-N phase	Structure	Space group	Lattice constants (Å)	Card number
$TaN_{0.04}$	Cubic	l	a=10.09	14-0471
$TaN_{0.1}$	Cubic	Im3m	a=3.369	25-1278
Ta_4N	Orthorhombic	C	a=5.16, b=3.11, c=9.94	32-1282
$Ta_6N_{2.57}$	Hexagonal	P-31m	a=5.285, c=4.919	31-1270
Ta_2N	Hexagonal	$P6_3/mmc$	a=3.0445, c=4.9141	26-0985
$TaN_{0.8}$	Hexagonal	P-6m2	a=2.931, c=2.879	25-1279
TaN	Cubic	Fm3m	a=4.33	32-1283
TaN	Hexagonal	P6/mmc	a=5.1918(3), c=2.9081(2)	39-1485
Ta_3N_5	Orthorhombic	Cmcm	a=3.893, b=10.264, c=10.264	19-1291

Tantalum nitrides are widely studied for microelectronic applications including diffusion barrier layers between metals and silicon,[14-24] gate electrodes,[4,25-29] and passivation layers against copper oxidation.[30,31] TaN has also been investigated as a nonmagnetic interlayer in NiFeCo/TaN/NiFeCo nonvolatile magnetic random access memories (MRAM).[32] In addition to the microelectronic applications, tantalum nitride has been used as protective and hard coatings and in various sensors and actuators.[33,34] Another potential application of TaN is as a biomedical material, for example in artificial heart valves.[35]

2.1.2. Niobium nitride

As with tantalum nitride, several crystalline phases exist in the phase diagram of Nb-N.[36] Table II presents the phases listed in the JCPDS data file. The Nb-N system has been studied closely and no dielectric phase has been reported to exist.[36-39] Most studies related to NbN deal with its superconducting properties.[40-43] The superconductivity of NbN was found as long ago as 1941 by Justi *et al.*,[44] and the highest T_c measured for NbN compound is approximately 17.3 K.[45] Niobium nitride alloys, for example the Nb-Ti-N system, also show superconducting behavior.[46]

Table II. Crystal structures and corresponding JCPDS data cards for Nb-N phases.

Nb-N phase	Structure	Space group	Lattice constants (Å)	Card number
$Nb_{4.62}N_{2.14}$	Hexagonal	-	-	30-0869
NNb_2	Hexagonal	-	-	40-1274
Nb_4N_3	Tetragonal	-	a=4.382, c=4.316	20-0803
$Nb_4N_{3.92}$	Cubic	-	-	34-0337
$NbN_{0.95}$	Hexagonal	P63/mmc	a=2.968, c=5.535	25-1361
NbN	Hexagonal	P63/mmc	a=2.96, b=2.96, c=11.27	20-0801
δ-$NbN_{1.000}$	Cubic	Fm3m	a=4.3927	38-1155
NbN	Cubic	-	-	43-1420
NbN	Cubic	-	-	43-1421
NbN	Hexagonal	-	-	14-0547

The superconducting nature of NbN has been exploited in low temperature superconducting electronics such as tunnel junctions[47,48] and nano-structured single photon detectors.[49-51] Good mechanical properties such as hardness and toughness make it a suitable material for wear protective coatings.[52-54] The mechanical properties of NbN have been enhanced by depositing TiN/NbN,[55-57] Si_3N_4/NbN,[58] W/NbN,[59] and TaN/NbN[60] superlattice films. The chemical inertness of NbN makes it a good material for corrosion protective coating.[61] NbN has also been studied as a possible cathode material in vacuum microelectronic devices.[62,63] Furthermore, the chemical inertness, high melting point,[64] and low resistivity[65,66] are desired properties for a diffusion barrier in microelectronic devices. The diffusion barrier properties of NbN have been little

studied, however. Niobium nitride has also been investigated as a catalyst for thiophene hydrodesulfurization.[67]

2.1.3. Molybdenum nitride

As indicated in Table III nitrides with many different molybdenum oxidation states are known. No dielectric phases seem to appear. The MoN phase is thermodynamically relatively stable as the melting point is 1750 ^{o}C, but Mo_2N has been observed to decompose at 790 ^{o}C.[68] Molybdenum nitride films have very low resistivity values down to 100 μΩ cm.[69,V] The hexagonal MoN phase has also been reported to show superconductivity, with T_c up to 12 K.[70]

Table III. Crystal structures and corresponding JCPDS data cards for Mo-N phases.

Mo-N phase	Structure	Space group	Lattice constants (Å)	Card number
$Mo_{16}N_7$	Tetragonal	-	a=8.41, c=8.05	23-1256
Mo_2N	Tetragonal	l41/amd	a=4.21, c=8.06	24-0768
Mo_2N	Tetragonal	l41/amd	a=4.188, c=8.048	25-1368
γ- Mo_2N	Cubic	Pm3m	a=4.163	25-1366
MoN	Hexagonal	P63/mmc	a=5.725, c=5.608	25-1367

Molybdenum nitrides have attracted considerable attention because they show excellent catalytic properties, resembling those of noble metals in many hydroprosessing reactions.[71,72] Molybdenum nitrides have been applied in hydrodesulfurization,[73,74] hydrodenitrogenation,[75] hydrogenation of alkadienes,[76] ammonia synthesis,[77] and catalytic decomposition of ammonia[78] and hydrazine[79]. Both MoN and γ-Mo_2N phases exhibit high bulk modulus[80,81] and both have been studied as hard coatings.[82,83] Also, the ternary phases Mo-Ti-N[84,85] and $MoSi_2N_x$[86] exhibit good mechanical properties. Diffusion barrier properties of molybdenum nitride films have also been investigated.[87-89]

2.1.4. Diffusion barrier applications

Copper has already partly replaced aluminum and aluminum alloys in the future ultra large scale integration microelectronic (ULSI) devices. In many respects, the properties of copper are superior to those of aluminum: lower bulk resistivity, higher melting point, and higher electromigration resistance. However, as copper readily diffuses into insulators and silicon and forms copper silicides, destroying the device in the process, an effective diffusion barrier is essential.

Barrier materials must meet tough requirements (Fig. 2).[90] Diffusion of metals and silicon through the barrier need to be efficiently prevented; the barrier material may not react with the metal or the semiconductor; it must have good adhesion to the adjacent materials; and it must be stable during both manufacturing and operation of the device. Since diffusion takes place primarily along grain boundaries, amorphous or nanocrystalline microstructures are preferred for the barrier material.[3] Even ultra thin barrier layers must perform effectively, as the barrier thickness is expected to decrease from 12 nm in the 100 nm node (year 2003) to 2.5 nm in the 22 nm node by the year 2016.[2]

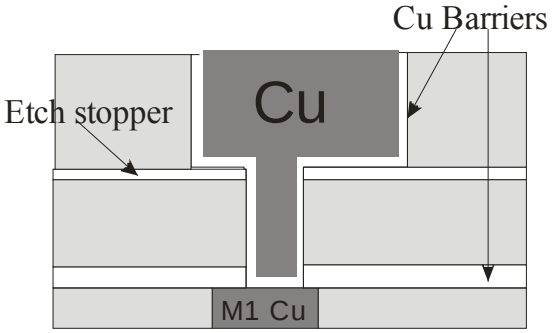

- high thermal stability to the surrounding materials
- enhanced resistance to thermal and mechanical stresses
- excellent adhesion to the adjacent materials
- low resistivity
- preferably amorphous
- deposited at low temperatures

Figure 2. Main requirements for an ideal barrier material (after references 3 and 91).

Transition metal nitrides, metal silicides, and metal-silicon-nitrides are widely used and studied as diffusion barriers. Until recently, titanium nitride was the most intensively studied material, but lately tantalum nitride has attracted much interest. Tantalum nitride offers superior barrier properties: it has a high melting

point and it is very hard, highly conductive, and thermodynamically very stable with respect to copper because it does not form compounds with it.[91] The grain boundaries of TaN are disordered, which should effectively prevent copper diffusion. Barriers could be an application for niobium and molybdenum nitrides as well as these materials possess similar properties to the tantalum nitride. The barrier properties of niobium and molybdenum based materials have been little studied.

2.1.5. Gate electrode applications

Metal oxide semiconductor field effect transistor (MOSFET) is the main component in integrated circuits such as microprocessors and semiconductor memories. The main parts of a MOSFET are source, drain, gate, gate oxide, and channel. Figure 3 shows a schematic diagram of an n-channel metal oxide semiconductor (NMOS) device where the substrate is a p-type semiconductor into which two n^+ regions, the source and the drain are formed.[92] A p-channel MOS (PMOS) can be formed changing the substrate to an n-type semiconductor, and the source and drain to p^+ regions. One PMOS and one NMOS device form a complementary metal oxide semiconductor (CMOS) structure.

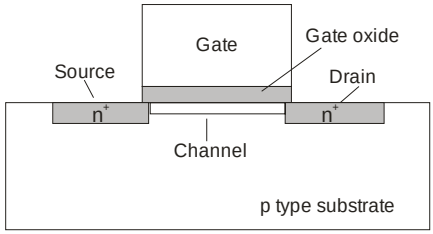

Figure 3. Schematic diagram of an NMOS device (after reference 119).

As the dimensions of devices are continuously scaled down, traditional materials can no longer meet the requirements. So far, silicon dioxide based materials have been used as gate oxides, but when the thickness of the gate oxide falls below 1.2 nm, tunneling currents will become too high.[2] The most widely studied high-k materials to replace SiO_2-based materials are aluminum oxide,[93,94] zirconium

oxide,[95,96] and hafnium oxide,[97,98] all of which have much higher permittivity than SiO_2. As the gate oxide thickness decreases, the capacitance associated with the depletion layer in the polycrystalline silicon gate electrode at the interface with the gate oxide becomes significant. It is expected, therefore, that metal gates will replace polycrystalline silicon, as this will eliminate the gate depletion. However, the requirements for the metal gate are tough. The material has to be stable during manufacturing and operation of the device and it must not react with materials under or above, the impurity content should be low, and, most importantly, the material must have an appropriate work function value.[2] The optimal work function for NMOS devices is 0.2 eV below the conduction band edge of silicon, while for PMOS devices it is 0.2 eV above the valence band edge of silicon.[99] This means that, the work functions for the n-type and p-type gates should be approximately 4 and 5 eV. TaN and Ta-Si-N are considered promising materials to replace polycrystalline silicon in CMOS devices as they have high thermal stability and are inert to reaction with other materials.

2.2. Atomic layer deposition

Atomic layer deposition (ALD) is a surface-controlled method for the deposition of films from gas phase.[5-7,100] In ALD the gaseous reactants are alternately pulsed to the substrates, and between the reactant pulses the reactor is purged with an inert gas. When the experimental conditions are properly chosen, the film growth proceeds via self-limiting saturative surface reactions, which makes it easy to control the film thickness and results in excellent conformality and large area uniformity. Besides these advantages in film properties, the separate pulsing of precursors allows the use of highly reactive precursors.

Figure 4 shows a schematic representation of a basic ALD cycle in a process with two precursors.[7] In this example, ZnS film is deposited with use of $ZnCl_2$ and H_2S as precursors. First $ZnCl_2$ is pulsed into the reaction chamber and a monolayer of the precursor is chemisorbed on the substrate. Next the excess of the precursor is purged away with an inert gas. The second precursor H_2S is pulsed into the reactor and reacts with the chemisorbed $ZnCl_2$, forming a ZnS layer on the substrate and HCl gas as a byproduct. The HCl gas and excess H_2S are then purged with an inert carrier gas. The second purge completes one deposition cycle. The desired film thickness is obtained by repeating the deposition cycle an appropriate number of times. In the ideal case, a complete

monolayer is formed in every deposition cycle and no impurities are introduced to the film. In practise, the deposition reactions seldom form a complete monolayer and some precursor decomposition may occur.

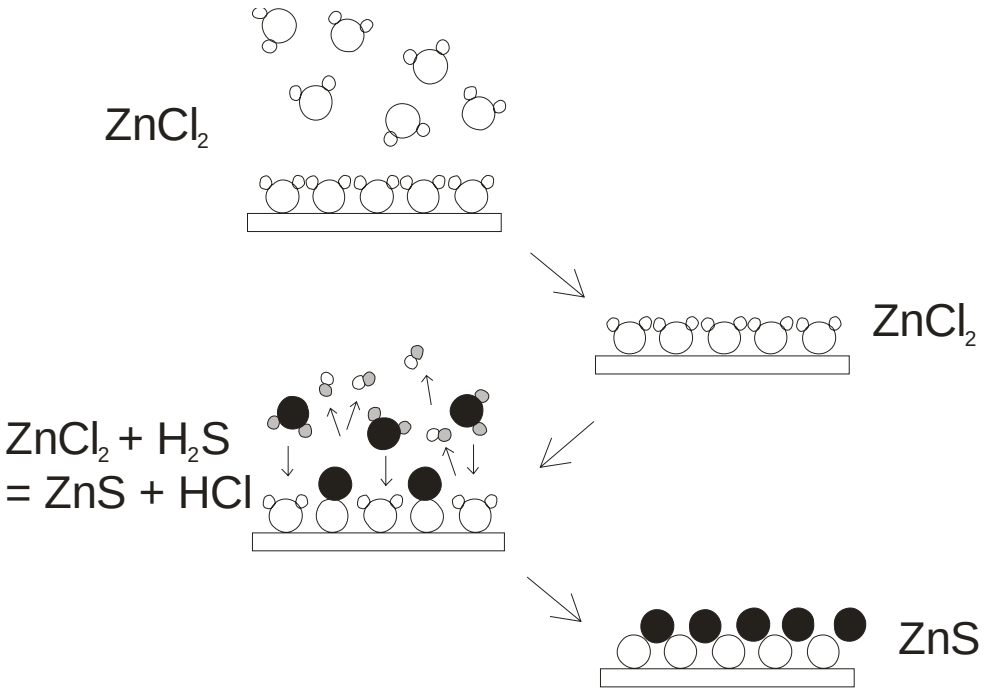

Figure 4. A schematic representation of the basic principle of the ALD process showing the growth of ZnS film from $ZnCl_2$ and H_2S (after reference 7). For clarity the relative sizes of the Zn and S atoms have been enlarged.

The good quality and excellent conformality of the films deposited by ALD make it a promising technique for a variety of microelectronic applications.[2] Films deposited by ALD typically contain less impurities and have lower deposition temperatures than films deposited by other chemical vapor deposition (CVD) methods. In high aspect ratio structures, the excellent conformality[101] makes the ALD technique superior to physical vapor deposition (PVD) methods.

2.3. Deposition and properties of tantalum nitride films

First some selected examples of tantalum nitride PVD and CVD (Table IV) literature are introduced. After that the literature of tantalum nitride and tantalum-silicon-nitride films deposited by the ALD technique is reviewed (Table V). The diffusion barrier and gate electrode properties of tantalum nitride and tantalum-silicon-nitride films are discussed.

2.3.1. Tantalum nitride films deposited by PVD and CVD

Physical vapor deposition (PVD) methods, especially sputtering, have been widely used to deposit tantalum nitride films.[14-17,30,102] The films do not contain impurities, they have low resistivity, and the desired phase is easy to obtain. However, films deposited by sputtering have modest step coverage, limiting their use in the modern microelectronic devices. More conformal films can be deposited with CVD techniques (Table IV). On the other hand, different problems are related to the CVD techniques. In the conventional CVD the temperatures needed are quite high (> 800 ^{o}C for $TaCl_5$-N_2-H_2 process),[103,104] the halogen impurities are easily incorporated, and it is difficult to obtain the desired tantalum nitride phase.[11] Attempts have been made to solve these problems by applying methods such as metal-organic CVD (MOCVD) and plasma-assisted CVD (PACVD).

In order to lower the deposition temperatures tantalum pentabromide ($TaBr_5$) has been studied as an alternative metal precursor to tantalum pentachloride.[17,105,106] Tantalum pentabromide has a lower heat of formation (-599 kJ/mol) than tantalum pentachloride (-858 kJ/mol) which implies that $TaBr_5$ should decompose at lower temperature than $TaCl_5$.[17] Kaloyeros *et al.*[105] deposited TaN_x films with a low temperature CVD method from $TaBr_5$, NH_3, and H_2. The deposition temperature was varied between 350 and 500 ^{o}C. The lowest resistivity (5 000 μΩ cm) was obtained at 500 ^{o}C. According to the X-ray diffraction (XRD) results, the films consisted of a mixture of TaN and Ta_3N_5 phases. The carbon, oxygen, and bromide contents were below 1 at. % each. Kaloyeros *et al.*[17] also reported TaN_x films deposited by the same method and with the same precursors but with lower resistivities. The films were deposited at 425 ^{o}C and contained very few impurities. The resistivity was only 2 500 μΩ cm, even though these films, too, consisted of a mixture of TaN and Ta_3N_5 phases.

Very low resistivities were obtained with plasma-assisted CVD and $TaBr_5$, N_2, and H_2 as precursors.[106] The TaN films deposited at temperatures between 350 and 450 ^oC contained less than 3 at. % of bromine and had resistivities as low as 150 μΩ cm.

Metal-organic precursors have been used to deposit tantalum nitride films. When pentakis(dimethylamido)tantalum (PDMAT, $Ta(NMe_2)_5$) and NH_3 were used as precursors in low temperature CVD, the films were yellowish and transparent indicating that they were of the dielectric Ta_3N_5 phase.[107] When the deposition method was remote plasma assisted MOCVD, the cubic TaN phase was obtained with PDMAT as a precursor.[108,109] Han *et al.*[108] used hydrogen plasma to reduce PDMAT. The amorphous films deposited at 200-350 ^oC were dark brown and the lowest resistivity was approximately 2 000 μΩ cm. The films were nitrogen-rich and carbon-rich. XPS studies indicated that most of the carbon was in the form of carbide. Cho *et al.*[109] used NH_3 plasma in addition to H_2 plasma. When NH_3 plasma was used the carbon content decreased markedly with the increasing deposition temperature, but with H_2 plasma it increased when deposition temperature was increased.

Besides PDMAT, its ethyl analogue, pentakis(diethylamido)tantalum (PDEAT, $Ta(NEt_2)_5$), has been used to deposit tantalum nitride films.[18,19] Cho *et al.*[18] deposited TaN_x films using PDEAT with and without NH_3 at temperatures between 300 and 375 ^oC. Although the films were highly nitrogen–rich, the authors suspected that they were TaN phase rather than Ta_3N_5 as the resistivities were fairly low (12 000 μΩ cm with NH_3 flow rate of 25 sccm) and the XRD results clearly indicated the existence of the TaN phase. Both carbon contents and resistivities were dependent on the addition of ammonia. The films were nearly carbon-free when the flow rate of ammonia was 25 sccm, but, the carbon content in the absence of ammonia was over 30 at. %. Although the addition of ammonia lowered the carbon content and resistivity, it also drastically lowered the step coverage. To improve the quality of films deposited from PDEAT, Im *et al.*[19] supplied nitrogen or argon ion beams during the deposition. The oxygen content in the films was below the detection limit of Auger electron spectroscopy (AES), but the films contained 20 to 30 at. % of carbon. The ion bombardment increased the film densities markedly, from 5.85 g/cm^3 (obtained with the thermal CVD) to 8.26 g/cm^3 for the Ar bombarded films. The film densification was reflected in the resistivity values. The resistivities obtained with both the

nitrogen and argon ion beams were lower than those obtained with thermal CVD (10 000 μΩ cm at 350 °C). The lowest resistivity of the TaN_x films was about 600 μΩ cm, which was obtained at 350 °C by using argon ion beam.

Table IV. Precursors, reaction temperatures, and properties of Ta-N CVD films.

Precursors	**Deposition temperature (°C)**	**Crystallinity**	**Properties**	**References**
$TaCl_5$-N_2-H_2	> 800 °C	TaN, Ta_2N	not reported	103,104
$TaCl_5$-N_2 plasma	600-650	Ta_2N_3	not reported	11
$TaBr_5$, NH_3, and H_2	350-500	TaN, Ta_3N_5	2 500 μΩ cm (425 °C)	17,105,106
$TaBr_5$, N_2, H_2 and plasma	350-450	TaN	150 μΩ cm, < 3 at% Br	106
PDMAT-NH_3	200-400	Ta_3N_5	N:Ta ~ 1.7, > 1 x 10^6 μΩ cm	107
PDMAT- H_2 plasma	200-350	amorphous	2 000 μΩ cm, N and C rich films	108
PDMAT- NH_3 plasma	200-350	≥ 300 °C: TaN < 300 °C: amorphous	200 °C: N:Ta ~ 0.9, C:Ta ~ 1.5 300 °C: N:Ta ~ 1.1, C:Ta ~ 0.51 4 000 μΩ cm – 1 Ω cm	109
PDEAT	300-375	TaN	> 30 at% C, good conformality	18
PDEAT-NH_3	300-375	TaN	no C, bad conformality	18
PDEAT- N-ions or Ar-ions	275-400	not reported	20-30 at% C, 600 μΩ cm (350 °C)	19
TBTDET	450-650	TaN	450 °C: 13 000 μΩ cm, ~ 100 % step coverage 650 °C: 900 μΩ cm, ~ 25 % step coverage	110,111
$(Et_2N)_3Ta{=}NEt$	500-650	TaN	carbon rich films	112
$Ta(NEt_2)_2(NCy_2)_2$-NH_3	340	amorphous	2.5 ± 0.1 x 10^5 μΩ cm density 6.6-7.0 g/cm^3	113
$[TaCl_2(N^tBu)(NH^tBu)$-$(NH_2{}^tBu)]_2$	500-600	Ta_3N_5	yellow-brown coloured	114
$[TaCl_2(NNMe_2)(NHNMe_2)$ $-(NH_2NMe_2)]_n$	400-600	TaN	Ta:N ~ 1:1.1, 2.1 x 10^5 μΩ cm (600 °C)	114
$TaCl_5$-$NH(SiMe_3)_2$	400-580	≥ 550 °C TaN, < 550 °C amorphous	500 μΩ cm (550 °C), no chlorine	115

The strong double bond between tantalum and nitrogen in *tert*-butylimidotris(diethylamido)tantalum (TBTDET, $(Et_2N)_3Ta=N^tBu$) was expected to preserve the "TaN" portion of the precursor during the deposition process.[110,111] The resistivity decreased from about 13 000 μΩ cm to about 900 μΩ cm when the deposition temperature was increased from 450 to 650 °C. The films contained about 10 at. % of carbon and 5-10 at. % of oxygen. When the deposition temperature was 450 °C, nearly 100% step coverage was achieved but when the deposition temperature was increased to 650 °C the step coverage decreased to only 25%. In an earlier study, a similar precursor, ethylimidotris-(diethylamido)tantalum ($(Et_2N)_3Ta=NEt$), was used to deposit cubic TaN_x films between 500 and 650 °C.[112] The dark gray films with metallic shine were carbon-rich.

In the commonly used CVD precursors, tantalum predominantly exists in oxidation state +V. For the conductive TaN phase to be obtained, tantalum must be reduced to oxidation state +III. Lehn *et al.*[113] partly avoided the reduction problem by using Ta(IV) dialkylamido complex $Ta(NEt_2)_2(NCy_2)_2$. Shiny golden-brown films were deposited at 340 °C from $Ta(NEt_2)_2(NCy_2)_2$ and NH_3 by aerosol-assisted atmospheric pressure CVD method. According to Rutherford backscattering spectrometry (RBS), the films contained hydrogen and chlorine impurities, while the contents of carbon and oxygen were below the detection limit (<2-3 at. %). The chlorine contamination was probably due to incomplete purification of the dialkylamido complex. The composition of the amorphous films was approximately $TaN_{1.54}Cl_{0.04}H_{0.33}$ and the densities were in the range 6.6-7.0 g/cm^3. According to the XPS data, the average oxidation state of tantalum in the films was +IV, which explains the high resistivity values (2.5×10^5 μΩ cm).

Winter *et al.*[114] prepared single-source precursors for TaN by treating $TaCl_5$ with *tert*-butylamine or 1,1-dimethylhydrazine. A $[TaCl_2(N^tBu)(NH^tBu)(NH_2{}^tBu)]_2$ complex was formed in the reaction with *tert*-butylamine. According to XRD, the yellow-brown films deposited from this precursor at 500 to 600 °C had the Ta_3N_5 phase. 1,1-Dimethylhydrazine formed a fairly similar single-source precursor $[TaCl_2(NNMe_2)(NHNMe_2)(NH_2NMe_2)]_n$ and with it the desired TaN phase was obtained at deposition temperatures of 400-600 °C. The tantalum:nitrogen ratio of the silver-colored films was 1:1.1, and the oxygen content of the films was 6%

relative to tantalum. The resistivity of a film deposited at 600 ^{o}C was as high as 2.1 x 10^{5} μΩ cm.

Tantalum nitride films can also be deposited with use of other precursors with reducing ability besides ammonia. Parkin *et al.*[115] deposited TaN films by atmospheric pressure CVD method using $TaCl_5$ and 1,1,1,3,3,3-hexamethyldisilazane ($NH(SiMe_3)_2$, HMDS) as precursors. HMDS acted as both a nitrogen source and a reducing agent. Reflective silvery films were deposited at temperatures of 400-580 ^{o}C. The films deposited at and above 550 ^{o}C were crystalline with the TaN phase, while those deposited below 550 ^{o}C were amorphous. The film deposited at 550 ^{o}C had resistivity as low as 550 μΩ cm. No chlorine impurities were observed.

2.3.2. Tantalum nitride and tantalum-silicon-nitride films deposited by ALD

In the first study on tantalum nitride films deposited by ALD both TaN and Ta_3N_5 phases were obtained when $TaCl_5$ and NH_3 were used as precursors.[116] The process was only briefly described, and later Ritala *et al.*[117] studied the $TaCl_5$-NH_3 and $TaCl_5$-Zn-NH_3 processes more thoroughly. With the $TaCl_5$-NH_3 process, the films deposited were of the dielectric Ta_3N_5 phase. The films deposited at 300 ^{o}C or above contained only a few at. % of impurities whereas those deposited at 200 and 250 ^{o}C contained large amounts of chlorine, hydrogen, and oxygen. Above 300 ^{o}C the deposition rate was constant at approximately 0.23-0.24 Å/cycle, whereas at 200 ^{o}C it was as low as 0.12 Å/cycle. Use of Zn as an additional reducing agent gave the desired cubic TaN phase. The TaN films deposited at 500 ^{o}C contained only 0.1 at. % of chlorine, and no zinc or hydrogen was detected with time-of-flight elastic recoil detection analysis (TOF-ERDA) or with nuclear resonance broadening (NRB) technique. The resistivity was about 900 μΩ cm. The deposition rate decreased slightly with increasing deposition temperature, being 0.20 and 0.15 Å/cycle at 400 and 500 ^{o}C, respectively. This study clearly showed that the reducing power of NH_3 is too weak to reduce Ta(V) to Ta(III) and an effective additional reducing agent is needed to achieve TaN films.

Table V. Precursors, reaction temperatures, and properties of Ta-N ALD films.

Precursors	**Deposition temperature (°C)**	**Crystallinity**	**Properties**	**Refs**
$TaCl_5$-NH_3	200-500	≥ 400 °C: Ta_3N_5 < 400 °C: amorphous	200 °C: ~ 23 at% Cl, 200 Ω cm 500 °C: ~ 0.1 at% Cl, 0.5 Ω cm	116,117
$TaBr_5$-NH_3	400-500	Ta_3N_5	400 °C: 1.5 Ω cm 500 °C: 41 000 μΩ cm	I
$TaCl_5$-Zn-NH_3	400-500	TaN	400 °C: ~ 4 at% Cl, 500 °C: ~ 0.1 at% Cl, 9x 10^{-4} Ω cm	117
$TaBr_5$-Zn-NH_3	400-500	TaN	400 °C: 1 100 μΩ cm, 4 at% Br 500 °C: 1 000 μΩ cm, <1 at% Br	I
$TaCl_5$-DMHy	300-400	amorphous (Ta_3N_5)	300 °C: 14 at% Cl 400 °C: < 0.5 at% Cl	69
$TaCl_5$-TMA-NH_3	250-400	TaN	250 °C: 19 at% C, 14 at% Cl, ~ 22 000 μΩ cm 400 °C: 26 at% C, 4 at% Cl, 1 300 μΩ cm	I
$TaBr_5$-TMA-NH_3	250-400	TaN	250 °C: 11 at% Br, 64 000 μΩ cm 400 °C: 4 at% Br, 6 600 μΩ cm	I
$TaCl_5$-^{t}BuNH$_2$	350-500	TaN	350 °C: 1 at% C, 5 at% Cl, ~ 1 Ω cm 500 °C: 20 at% C, 3 at% Cl, 1 500 μΩ cm	II
$TaCl_5$-^{t}BuNH$_2$-NH_3	400-500	TaN	400 °C: 2 at% C, 2 at% Cl, 11 000 μΩ cm 500 °C: 11 at% C, 2 at% Cl, 1 900 μΩ cm	II
$TaBr_5$-^{t}BuNH$_2$	400-500	TaN	400 °C: 2 at% C, 6 at% Br, 80 000 μΩ cm 500 °C: 16 at% C, 2 at% Br, 1 300 μΩ cm	II
$TaBr_5$-^{t}BuNH$_2$-NH_3	400-500	TaN	400 °C: 1 at% C, 1 at% Br, 32 000 μΩ cm 500 °C: 7 at% C, 1 at% Br, 2 700 μΩ cm	II
$TaCl_5$-allylNH$_2$-NH_3	400	TaN	10-14 at% C, 8-10 at% Cl, 5-7 at% O, 18 000-41 000 μΩ cm	II
$TaCl_5$-H_2/N_2 plasma	100-400	TaN	N:Ta varied from 0.3 to 1.4, 5-10 at-% O, 350-400 μΩ cm	118,119
PDMAT-NH_3	275	TaN	N:Ta ~ 2, 2 at% C, 5 at% O	120
PEMAT-NH_3	250	amorphous	Ta:N ~ 4.2:5, 11at% O, 8-10 at% C, δ ~ 8.4 g/cm^3	122
PEMAT-NH_3-Ar plasma	250	amorphous	Ta:N ~ 1:1, 4 at% O, 3 at% C, δ ~ 11.6 g/cm^3	122

TBTDET-NH_3	250-260	amorphous	Ta:N ~ 1:1, 5-8 at.% C and O 500-1.38 x 10^8 μΩ cm	123,124 126
TBTDET-H_2 plasma	250-260	TaN/TaC	Carbon rich films, 250-400 μΩ cm	123,125 127
$TaCl_5$-H_2/N_2 plasma-SiH_4	not reported	nor reported	20 at% Ta, 25 at% N, 55 at % Si, < 1 000 μΩ cm	128
$TaCl_5$-TDMAS-NH_3	300-500	≥ 400 °C: TaN < 400 °C: amorphous	300 °C: 10 at% Cl, 3.5 at% Si 500 °C: < 1 at% Cl, 7.5 at% Si, < 10 000 μΩ cm	III

Even though Zn is an efficient reducing agent, even minor amounts of Zn impurities will cause severe problems if they diffuse into the silicon substrate. An alternative method for reducing Ta(V) is required, therefore. Recently, Juppo *et al.*[69] deposited films from $TaCl_5$ and 1,1-dimethylhydrazine (DMHy), the last a more reductive nitrogen source than ammonia. The radical formation enthalpies are 297 and 461 kJ/mol for DMHy and NH_3, respectively, indicating that ammonia is much more stable than DMHy. However, the amorphous films that were obtained seemed to be dielectric Ta_3N_5 rather than TaN because they were highly resistive and partly transparent. The deposition rate at 300 °C was rather good (0.3 Å/cycle).

Kim *et al.*[118] used the PEALD method to deposit TaN films. The deposition was accomplished by alternate exposures of the metal precursor $TaCl_5$ and the plasma of hydrogen and nitrogen mixture. The N/Ta ratio of the films increased from 0.3 to 1.4 with increasing nitrogen partial pressure. The cubic TaN phase was obtained with the N/Ta ratio between 0.7 and 1.3. The resistivity of the cubic TaN was typically 350-400 μΩ cm and the deposition rate was 0.24 Å/cycle. The chlorine contents and resistivities depended on the plasma exposure time. Reasonably low chlorine content and low resistivity were obtained only when the plasma exposure time exceeded 5 s. The films contained 5 to 10 at. % oxygen. The physical properties of these TaN films were studied in more detail in a later study. XRD patterns of PEALD TaN films on silicon were measured after rapid thermal annealing (RTA) up to a temperature of 1000 °C in He atmosphere.[119] New crystalline phases were not observed after RTA, which indicated that the TaN–Si interface had remained stable. In order to obtain more information about the stability of TaN films on Si and SiO_2, samples were annealed to temperatures between 800 and 1000 °C and analyzed by the medium energy ion scattering (MEIS) method. No intermixing of the TaN film and substrate was observed.

TaN_x films deposited by CVD methods from metal-organic precursors containing dialkylamido ligands or imido and dialkylamido ligands have shown promising properties, and recently these precursors have been used to deposit tantalum nitride films also by ALD method. Wu *et al.*[120] studied the properties and stability of very thin (1.5-10 nm) tantalum nitride films deposited at 275 °C from pentakis(dimethylamido)tantalum (PDMAT, $Ta(NMe_2)_5$), and ammonia. The films were nitrogen-rich as the N/Ta ratio was as high as 2. The films contained some carbon (2 at. %) and oxygen (5 at. %) impurities. Even the thinnest films (1.5 nm) were observed to consist of the TaN phase. The as-deposited films with thicknesses of 5 and 10 nm possessed a nanocrystalline structure and their average crystallite size was approximately 4 nm. When the films were thermally annealed at 700 °C the crystallite size increased, but no phase changes occurred. The continuity and morphology of tantalum nitride films deposited from PDMAT and NH_3 have been studied by first exposing the deposited film to HF and then analyzing the sample by cross-sectional SEM.[121] This testing procedure indicated that even films less than 2 nm thick were continuous and free from pinholes.

Both conventional ALD and plasma-assisted ALD (PAALD) methods have been used to deposit tantalum nitride films at 250 °C with pentakis-(ethylmethylamino)tantalum (PEMAT) and ammonia as precursors.[122] The films deposited by conventional ALD were nitrogen-rich (Ta:N ~ 1:1.2) and contained considerable amounts of carbon (8-10 at.%) and oxygen (11 at. %) impurities. Use of the PAALD method instead resulted in decreased amount of nitrogen (Ta:N ~ 1:1) and impurities (3 at. % C, 4 at. % O) in the films. The films deposited by PAALD were also of higher density (~ 11.6 g/cm^3) than those deposited by conventional ALD (~ 8.4 g/cm^3). The sheet resistance value of the PAALD films remained stable when the film was exposed to air. In contrast to this, the sheet resistance of the film deposited by conventional ALD continuously increased when under air exposure.

tert-Butylimidotris(diethylamido)tantalum (TBTDET) has been used as precursor for the deposition of TaN films both by conventional ALD[123,124] and by plasma enhanced ALD (PEALD)[123,125] methods at 250-260 °C. Ammonia was used as reducing agent with the conventional ALD method. The TaN films deposited by conventional ALD by Park *et al.*[123] were amorphous and the film resistivity increased with air exposure from 1.4 x 10^6 to 1.4 x 10^8 μΩ cm within 80 hours.

The deposition rate was reasonably high, 1.1 Å/cycle, but the density of the film was only 3.6 g/cm^3. Later van der Straten *et al.*[124] studied the same TBTDET–NH_3 process and obtained amorphous TaN films with resistivities ranging from just 500 to 1000 μΩ cm for 30-nm-thick films. The Ta:N ratio was close to 1:1 and the films contained 5 to 8 at. % of carbon and oxygen. The deposition rate was 0.4 Å/cycle, which is less than half of that reported by Park *et al.*[123] The lower rate was attributed to the longer purge times. The excellent conformality of the TaN films was confirmed in 100-nm-wide trench structures with 11:1 aspect ratio. The low deposition temperature (250 ^{o}C) also enabled the deposition of TaN films on low dielectric constant (low-k) material SILK^{TM} which does not tolerate high temperatures.[126]

The PEALD method relying on hydrogen radicals as reducing agents at 260 ^{o}C yielded TaN films from TBTDET.[123,125] The resistivity was 400 μΩ cm with no aging effect under exposure to air. However, the films contained considerable amounts of carbon (20 at. %). According to XPS, carbon was present in the films as both tantalum carbide and hydrocarbons. TaC has lower resistivity than TaN and this partly explains the low resistivity that was obtained. The deposition rate of PEALD films saturated to a level of 0.8 Å/cycle when the pulse time of TBTDET exceeded 2 s. The density of the PEALD TaN film was 7.9 g/cm^3. Cheng *et al.*[127] were able to deposit films with very low resistivity, 250 μΩ cm, from TBTDET and hydrogen radicals at 250 ^{o}C. The Ta:C:N ratio was approximately 2:2:1. The films were composed of polycrystalline TaN and TaC phases and the step coverage in a 90 nm trench was 80%.

Ta-Si-N films have also been deposited by the PEALD method.[128] The precursors were $TaCl_5$, SiH_4, and nitrogen/hydrogen plasma. The Ta-Si-N films had a resistivity below 1 000 μΩ cm. The amorphous films contained 20 at. % tantalum, 25 at. % nitrogen, and 55 at. % silicon.

2.3.3. Diffusion barrier properties of tantalum nitride and tantalum-silicon-nitride films

Typically, in the study of barrier properties, a barrier layer is deposited on a silicon substrate and covered with a layer of copper. After the sample is annealed, several methods can be used to determine the barrier failure temperature. With XRD measurements, one can observe the formation of Cu_3Si which occurs when copper reacts with silicon. An increase in sheet resistance also indicates the failure of the barrier layer. The so called "Secco" etch method is considered more sensitive method. First the copper and barrier films are separately etched away, and then the copper silicide formed in silicon is removed with the "Secco" etch (one part of 0.15 M $K_2Cr_2O_7$ and two parts of HF). After etching Cu_3Si, microscopic pyramidal shaped etch pits can be observed on the surface of the silicon substrate. Other methods to study the barrier failure temperature are Auger electron spectroscopy (AES) depth profiles, Rutherford backscattering spectroscopy (RBS), transmission electron microscopy (TEM), synchrotron x-ray diffraction, optical scattering, sheet resistance measurements during thermal annealing of the sample, and scanning electron microscopy (SEM).

Electrical tests are the most accurate way to determine barrier performance. The capacitance-voltage (C-V) measurements performed on MOS capacitor structures before and after themal annealings are a simple way to observe barrier breakdown. Changes in the C-V curves imply barrier failure, as the diffused Cu atoms form deep donor levels in Si and act as generation and recombination centers, and the low-frequency C-V profile is detected in high-frequency conditions.[129] In addition to elevated temperatures the diffusion barrier should remain stable under an electric field. This can be studied, for example, with bias temperature stressing (BTS). First, MOS capacitor structures are formed and then an electric field is applied to the capacitor at elevated temperature. The C-V curves of the stack are measured before and after the stressing and the shift in the curve show the injection of mobile charge. A shift toward negative voltages is indicative of injection of positive charge, which in this case is the amount of diffused copper ions.

Diffusion barrier properties and failure mechanisms of PVD and CVD tantalum nitride and tantalum-silicon-nitride films have been fairly widely studied but will

be discussed here only briefly. Diffusion barrier properties of ALD tantalum nitride films have been less fully examined. In a recent study on PEALD TaN films, it was observed that the failure temperature of the barrier against Cu diffusion is relatively comparable to that of PVD TaN.[130] Peng *et al.*[131] integrated an ALD TaN barrier into the 90-nm generation Cu dual damascene technology with low-k dielectrics (k=3.0). The TaN barrier showed promising reliability performance in electromigration, stress migration, and bias temperature tests. Also, Chung *et al.*[132] found ALD TaN barriers with thicknesses below 10 Å to resist the diffusion of copper. The effective line resistivity of these highly nitrogen-rich (almost Ta_3N_5) films were below 2.1 μΩ cm for 0.1 μm line width.

Barrier properties have been studied in more detail for the PEALD TaN films deposited from $TaCl_5$ with nitrogen and hydrogen plasma at 300 ^oC.[119] Barriers with thicknesses 2.5, 5, and 12.5 nm were deposited on silicon and covered with a 200-nm-thick PVD copper layer. The samples were annealed in helium atmosphere from 100 to 1000 ^oC at a temperature ramp rate of 3 ^oC/s. During the annealing the samples were analyzed by synchrotron XRD, optical scattering, and measurement of the sheet resistances. The results obtained with the PEALD TaN films were compared with the results of PVD TaN films and found to be quite similar. It was further calculated that the PEALD TaN film with a thickness of 50 nm would have failed at 700 ^oC if isothermal annealing had been used.

The barrier performance of ALD TaN_x films deposited from TBTDET and NH_3 has been studied, too.[133,134] The Cu/TaN_x/Si samples were annealed in forming gas, after which the copper layer was etched selectively and the samples were analyzed by RBS to study the copper diffusion. A TaN_x barrier with thickness of 6 nm was observed to remain stable after annealing at 550^oC, while breakdown was noted after annealing at 600 ^oC. The triangular voltage sweep (TVS) method, where Cu/TaN_x/SiO_2/n-Si/Al stacks were first bias-voltage stressed and then the voltage was ramped, was used to determine the density of mobile charges diffused through the barrier into the underlying dielectric. With the bias of 20 volts at a stress temperature of 150 ^oC, no copper diffusion was observed with the 6-nm-thick TaN_x barrier. Copper diffusion was observed when the stress temperature was increased to 200 ^oC. Also Cheng *et al.*[127] studied the barrier performance of TaN_x films deposited from TBTDET and NH_3. According to the RBS data the 5-nm-thick TaN_x barrier remained stable after annealing in argon at 550 ^oC but failed at 650 ^oC. The TaN_x films deposited with PEALD from

TBTDET possessed similar barrier properties to the films deposited by thermal ALD.[127]

The stability of 10-nm-thick TaN films deposited by conventional ALD and plasma-assisted ALD methods from PEMAT and NH_3 has been studied by measuring the sheet resistance and XRD data of the annealed samples.[122] The Cu/TaN/SiO_2/Si stacks were annealed under nitrogen atmosphere for 30 minutes at different temperatures. The sheet resistance was observed to increase rapidly after the annealing at 700 ^oC both when ALD and when PAALD TaN films were used as barriers. The formation of $Cu_3Ta_{11}O_{30}$ phase was observed by XRD after annealings at 700 and 800 ^oC with the ALD and PAALD TaN films, respectively.

Min *et al.*[14] have reported the barrier properties of reactively sputtered TaN and Ta_2N films. The diffusion barrier tests indicated that two different mechanisms were responsible for the failure of the barrier. The failure mechanism in the case of Cu/TaN/Si structure is the diffusion of Cu through the barrier layer resulting in the formation of crystalline defects and Cu_3Si precipitates in the Si substrate. When Ta_2N was used as the barrier layer the predominant failure mechanism was the chemical reaction between the barrier layer and the Si substrate. The ternary phase diagram of Ta, N, and Si, based on the Gibbs free energy data at 627 ^oC, shows that tantalum nitrides are not thermodynamically stable in contact with silicon. The authors suggest that the reaction between Ta_2N and Si occurs at much lower temperatures than the reaction between TaN and Si. The barrier failures of Ta_2N and TaN occurred at 700 and at 750 ^oC, respectively, as judged from the sheet resistance measurements, XRD, AES depth profiles, and Secco etch pit observations.

In another study on sputter deposited Ta_2N films, the main reason cited for the barrier failure was the diffusion of Cu through the barrier and the formation of Cu_3Si.[15] No reactions between the barrier layer and the Si substrate were observed. The barrier properties of Ta_2N films of different thickness were studied by sheet resistance measurements and XRD. The barrier failure temperature was found to increase from 650 to 725 and 775 ^oC when the film thickness was increased from 10 to 50 and 100 nm, respectively.

Barrier properties of sputtered TaN films have also been studied with low-k materials. Wu *et al.*[16] examined the stability of Cu/TaN/PAE-2/Si structures.

PAE-2 (poly(arylene ether)) is a low-k organic polymer material which is thermally stable up to 450 ^{o}C. The thermal stability was evaluated from the time-zero dielectric breakdown of PAE-2. The sputtered TaN was observed to be an effective barrier up to 450^{o}C.

Kaloyeros *et al.*[17] compared the barrier properties of 55-nm-thick tantalum nitrides deposited by inorganic low temperature thermal CVD method with sputter deposited TaN films of the same thickness. The CVD films were deposited at 425 ^{o}C from tantalum pentabromide with ammonia and hydrogen as coreactants. Both the CVD and PVD tantalum nitrides were nitrogen-rich in composition. The CVD TaN_x ($x \sim 1.8$) began to fail above 550 ^{o}C (according to the etch pit tests), while the PVD TaN_x ($x \sim 1.7$) showed thermal integrity up to the highest temperature tested, 650 ^{o}C. The differences in the thermal behavior were suspected to be due to differences in film microstructures and crystalline phases, or in the location of the excess nitrogen within the film matrix. The CVD films were amorphous up to 600 ^{o}C, and above that temperature the film crystallized predominantly to the Ta_3N_5 phase. However, the PVD films were nanocrystalline and only minor changes in the grain size were observed after annealings. Additionally, in the cubic PVD TaN films the excess nitrogen was expected to be located in the grain boundaries.

The barrier performance of TaN_x films deposited by the metal-organic CVD (MOCVD) method from PDEAT with and without ammonia has also been studied.[18] With ammonia flow rates of 0 and 10 sccm 50-nm-thick barriers failed at 550 ^{o}C. A TaN_x barrier film deposited with higher NH_3 flow rate of 25 sccm failed at 600 ^{o}C. The barrier failure was evident as the formation of etch pits on the Si surface. The authors suspected that the slight improvement in the barrier property with higher ammonia flow rate might have been due to a change in the film microstructure, which became more crystalline when ammonia was added. TaN films, 50-nm-thick, deposited from PDEAT, either by thermal decomposition or by simultaneous ion bombardment of the growing film surface with nitrogen or argon ions, have been evaluated as barriers between Cu and Si.[19] The TaN film deposited by thermal decomposition without ion bombardment was reported to fail at 600 ^{o}C, while the ion bombarded films failed at 650 ^{o}C according to the XRD analysis. It was considered that the slightly improved barrier properties of the ion bombarded films were a consequence of the increase

in film density, which was only 5.85 g/cm^3 for the thermal CVD films, but 7.65 and 8.26 g/cm^3 for the nitrogen and argon ion bombarded films, respectively.

The barrier properties of PVD Ta-Si-N films have been studied extensively.[20-24] The failure mechanism has been described as the diffusion of copper through the barrier layer and the formation of copper silicides. The barrier failure temperatures of barriers of different thicknesses varied from 400 to 900 ^{o}C.

2.3.4. Gate electrode properties of tantalum nitride and tantalum-silicon-nitride films

Gopalan *et al.*[25] studied transistors with hafnium silicate gate dielectrics (equivalent oxide thickness (EOT) of 12.5-14 Å) and sputtered TaN gate electrodes. The authors reported excellent electrical stability of the Hf-silicate with the TaN metal gate after rapid thermal anneal (RTA) in N_2 ambient at 1000 ^{o}C. The capacitance-voltage (C-V) characteristics were good and hysteresis was almost negligible (< 10 mV). Good thermal stability of sputter deposited TaN gate electrodes in TaN/HfO_2/p-Si structures under high temperature annealings has also been reported by Choi *et al.*[135]

MOS capacitors have been prepared by depositing ALD TaN/PVD Ta metal electrodes on MOCVD HfO_2 and Hf_xSi_yO dielectrics.[136] The ALD TaN was deposited at 290 ^{o}C and the value for a 40 Å TaN/Ta on HfO_2 was 4.7 ± 0.05 eV. When the thickness of TaN was increased to 80 Å, a 100-mV flat band voltage (V_{fb}) shift was observed, which was considered to be due to a shift of the work function. This kind of V_{fb} shift was not found with Hf_xSi_yO. For the 40 Å TaN/Ta stack on Hf_xSi_yO, the work function was estimated to be 4.6 ± 0.05 eV. The Ta/TaN/HfO_2 structures were annealed in forming gas at 450 ^{o}C and were observed to be of good stability.

The physical and electrical properties of sputtered TaN and Ta-Si-N on HfO_2 gate dielectrics were recently reported.[26] In an inert ambient, the W/TaN/HfO_2 gate stacks were stable up to 900 ^{o}C, but some Hf and Ta interdiffusion was observed above that temperature. In the case of Ta-Si-N/HfO_2/Si gate stacks, the metal gate–dielectric interface was stable up to 1025 ^{o}C in an inert ambient and the work function of Ta-Si-N was independent of the N content in the 20-40 at.

% range. The TaN and Ta-Si-N films had similar work functions (approximately 4.4 eV) after the gate stacks had been annealed above 900 ^{o}C.

Also Suh *et al.*[4,27,28,137,138] have studied the electrical characteristics and thermal stability of sputtered Ta-Si-N films on silicon dioxide. The work function was measured after annealing the W/Ta-Si-N/SiO_2/p-Si stacks in forming gas at 400 ^{o}C for 30 min. The work function of Ta-Si-N varied between 4.19 and 4.27 eV as the N content in the films varied.[4] These work function values are appropriate for the n-type MOSFETs. The thermal stability of the Ta-Si-N/SiO_2/p-Si stacks was studied by exposing the samples to RTA in Ar ambient. EOT values were measured from C-V curves and the gate leakage currents were evaluated as a function of the annealing temperature.[28] The Ta-Si-N gates showed good stability on SiO_2 even up to 1000 ^{o}C with negligible change in EOT and no degradation of the C-V curves. However, it was also observed that, after 900 ^{o}C anneal, the work function of the Ta-Si-N films increased to approximately 4.8 eV.[27,138] The increase was attributed to the formation of a disilicide reaction layer at the interface of the electrode and the dielectric.

2.4. Deposition and properties of niobium nitride films

Deposition of niobium nitride films by PVD methods including sputtering,[40,47,50-52] ion beam assisted deposition (IBAD),[62,63,139] pulsed laser deposition (PLD),[39,42] and vacuum cathodic arc deposition[140] are widely reported. The films deposited by CVD-based methods exhibit better conformality than those deposited by PVD methods and are presented in Table VI. Conventional high temperature CVD methods have been used to deposit niobium nitride films. Oya and Onodera deposited superconducting niobium nitride films by reacting gaseous $NbCl_5$ with NH_3 and H_2 gases at atmospheric pressure in a fused silica reaction tube at substrate temperatures above 900 ^{o}C.[141-144] Niobium nitride films with various phases have also been deposited from the reactant gas mixture consisting of $NbCl_5$, N_2, H_2, and Ar at substrate temperatures of 900 ^{o}C and above.[145-147]

Table VI. Precursors, reaction temperatures, and properties of Nb-N CVD and ALD films.

Precursors	**Deposition temperature (°C)**	**Crystallinity**	**Properties**	**References**
CVD processes:				
$NbCl_5$-NH_3-H_2	> 900	NbN, Nb_4N_5	T_c up to 15.75 K	141-144
$NbCl_5$-N_2-H_2-Ar	> 900	Nb_2N, NbN, Nb_4N_3		145-147
$Nb(NEt_2)_4$-NH_3	200-425	not reported	N/Nb ~ 1.35 H/Nb ~ 1.15 (200 °C) H/Nb ~ 0.65 (300 °C) 10^3-10^4 μΩ cm	107,148, 149
$EtN=Nb(NEt_2)_3$	500-600	not reported	30 at% Nb, 15 at% N, 45 at% C, 10 at% O	149
$Nb(NMe_2)_5$-NH_3	200-400	not reported	N/Nb ~ 1.35 H/Nb ~ 1.15 (200 °C) H/Nb ~ 0.20 (400 °C) 10^3-10^4 μΩ cm	105
$Nb(NEt_2)_4$-N_2H_2 plasma	350-800	crystalline	13.5-3.2 at% O, ~10 at% C	151
$Nb(NEt_2)_4$-$Ta(NEt_2)_5$-NH_3	375-500	not reported	375 °C: 21 at% C, 19 at% O	150
$[N(CH_2CH_2NEt)_3]Nb=N^tBu$	750	not reported	11 at% O, 9 at% C	151
$NbCl_5$-$(SiMe_3)_2NH$	400-580	cubic NbN (≥ 550 °C)	500 μΩ cm (550 °C), no Cl	115
$[NbCl_2(N^tBu)(NH^tBu)(NH_2{}^tBu)]_2$	500-600	cubic NbN	C/Nb ~10 at% O/Nb ~ 6 at% 980 μΩ cm (500 °C)	114,152
$[NbCl_2(NNMe_2)(NHNMe_2)$-$(NH_2NMe_2]_n$	400-600	cubic NbN	O/Nb ~30 at%	114
ALD processes:				
$NbCl_5$-NH_3	300-500	cubic NbN	500 °C: <1 at% O, traces of Cl, 550 μΩ cm 400 °C: 15 at% Cl, >10 000 μΩ cm 300 °C: 24 at% Cl	65,66,69, 116,
$NbCl_5$-Zn-NH_3	500	cubic NbN	<1 at% O, traces of Cl, 200 μΩ cm	65,66
$NbCl_5$-DMHy	400	not reported	5 at% Cl, 2 900 μΩ cm	69

In an attempt to lower the deposition temperature, Fix *et al.*[107] used $Nb(NEt_2)_4$ and $Nb(NMe_2)_5$ compounds and ammonia as precursors. The amorphous films deposited between 200 and 400 ^oC from the two niobium dialkylamido complexes showed nearly identical properties and stoichiometry. The films were mirror-like, smooth, nonporous, and pinhole-free and showed good adhesion in the tape test. The nitrogen/metal ratio of the films was about 1.35, which suggests the composition Nb_3N_4. Although the films contained considerable amounts of hydrogen (H/Nb ~ 1.15 at 200 ^oC), resistivity values were moderate from 1 000 to 10 000 μΩ cm. In later NMR studies, the "$Nb(NEt_2)_4$" complex was found to consist of a mixture of two diamagnetic compounds (83 %) and one paramagnetic compound (17 %).[108,148] When the mixture was heated in a CVD reactor it converted entirely to ethylimidotris(diethylamido)niobium(V) [$EtN{=}Nb(NEt_2)_3$]. $NbN_xO_yC_z$ films were deposited with metal-organic CVD using the pure $EtN{=}Nb(NEt_2)_3$ as a precursor with and without ammonia.[149] The deposition temperatures were 300-425 ^oC when ammonia was used, and 500 to 600 ^oC without ammonia. The films deposited without ammonia contained 45 at. % carbon, whereas those deposited with ammonia contained approximately 20 at. %. Transamination reactions between $EtN{=}Nb(NEt_2)_3$ and NH_3 are the likely reason for the ammonia lowering the deposition temperature and carbon content of the films.

Gau *et al.*[150] deposited $Nb_xTa_{(1-x)}N_yO_mC_n$ films at 375 to 500 ^oC using $Nb(NEt_2)_4$ and $Ta(NEt_2)_5$ as precursors with ammonia as a reaction gas. The films deposited at 375 ^oC contained 19 at. % oxygen and their sheet resistances increased when the films were exposed to air. When the films were post-treated with NH_3 plasma the sheet resistance remained constant when the films were exposed to air. The use of NH_3 plasma post-treatment also lowered the oxygen content of the films. $Nb(NEt_2)_4$ has further been used as a precursor in the deposition of NbN films by the plasma-assisted, low pressure MOCVD process.[151] NbN films were deposited at temperatures from 350 to 800 ^oC with use of hydrazine plasma as a nitrogen source. The oxygen content decreased from 13.5 at. % to 3.2 at. % when the deposition temperature was increased from 550 to 750 ^oC. The carbon content remained fairly stable independent of the deposition temperature, being approximately 10 at. %. In the same study, niobium nitride films were also deposited from $[N(CH_2CH_2NEt)_3]Nb{=}N^tBu$ and hydrazine plasma. The films deposited at 750 ^oC contained 11 at. % of oxygen and 9 at. % of carbon.

Single-source precursors $[NbCl_2(N^tBu)(NH^tBu)(NH_2{}^tBu)]_2$ and $[NbCl_2(NNMe_2)(NHNMe_2)(NH_2NMe_2]_n$ have been used to deposit NbN films.[114] The imido-amido-amine complex $[NbCl_2(N^tBu)(NH^tBu)(NH_2{}^tBu)]_2$[152] gave smooth silver-colored cubic NbN films at deposition temperatures between 500 and 600 °C with good adhesion to glass and silicon substrates. The films contained small amounts of carbon and oxygen impurities. The resistivity of the film deposited at 500 °C was 980 μΩ cm. At deposition temperatures of 400 to 600 °C the $[NbCl_2(NNMe_2)(NHNMe_2)(NH_2NMe_2]_n$ complex gave relatively similar NbN films to those just described. The cubic NbN films were silver-colored and highly adherent. The films contained 30 % of oxygen relative to niobium.

Niobium nitride films were deposited by the atmospheric pressure CVD method from $NbCl_5$ and hexamethyldisilazane ($(SiMe_3)_2NH$) at 400-580 °C.[115] According to glancing angle XRD, the films deposited at and above 550 °C were crystalline, showing the cubic NbN structure. The films were chlorine-free, and those deposited at 550 °C had a resistivity of 500 μΩ cm.

ALD of niobium nitride films (Table VI) has mostly been studied at high temperatures with use of $NbCl_5$ and NH_3 as precursors, with and without an additional Zn pulse.[65,66,116] The NbN films deposited at 500 °C with and without zinc contained less than 1 at. % of oxygen and only traces of chlorine (0.01-0.04 at. % determined by TOF-ERDA). All the NbN films exhibited cubic structure. The resistivity values of the NbN films deposited with and without zinc were approximately 200 and 550 μΩ cm, respectively. The NbN films deposited at 300 and 400 °C without zinc had very low deposition rate and poor conductivity.[69] The film deposited at 400 °C had a resistivity above 10 000 μΩ cm and the sheet resistance of the film deposited at 300 °C could not even be measured. The films also contained a lot of chlorine, 24 at. % at 300 °C and 15 at. % at 400 °C. Instead of ammonia, 1,1-dimethylhydrazine (DMHy) has been used as a nitrogen source.[69] The films deposited from $NbCl_5$ and DMHy at 400 °C contained 5 at. % chlorine and had a resistivity of 2 900 μΩ cm.

2.5. Deposition and properties of molybdenum nitride films

Most molybdenum nitride films have been deposited by PVD methods, for example by sputtering[82,83,87-89,153] and ion beam assisted deposition (IBAD).[78,154] CVD-based methods have been applied more rarely. Depositions and properties of CVD films are summarized in Table VII. Fix *et al.*[155,156] deposited conductive molybdenum nitride films by atmospheric-pressure metal-organic CVD method. The deposition temperature was varied between 200 and 400 ^{o}C and the precursors were tetrakis(dimethylamido)molybdenum(IV), $Mo(NMe_2)_4$, and ammonia. The N/Mo ratio in the films was approximately 1.4-1.5, which implies a film stoichiometry close to Mo_2N_3. When the deposition temperature was increased from 200 to 400 ^{o}C the N/Mo stoichiometry remained relatively stable, but the H/Mo ratio decreased from 1.0 to 0.45. The carbon and oxygen contents were below the detection limit of Rutherford backscattering spectroscopy (RBS).

As well, metal halides have been used as precursors in the CVD of molybdenum nitride films. MoN films could be deposited from MoF_6 and NH_3 at temperatures from 500 to 700 ^{o}C when both H_2 and Ar were used as carrier gases.[157] Roberson *et al.*[158,159] applied $MoCl_5$ and NH_3 as precursors in a cold-wall vertical pancake-style reactor. The deposition temperatures ranged from 400 to 800 ^{o}C. The phase composition of the films was studied in detail by XRD. The films deposited at 400 ^{o}C contained both amorphous and cubic γ-Mo_2N phases. When the deposition temperature was increased, the relative content of γ-Mo_2N decreased and the hexagonal δ-MoN phase became more dominant. The maximum, 95% of δ-MoN and only 5% γ-Mo_2N, was obtained at a deposition temperature of 700 ^{o}C. When the deposition temperature was 800 ^{o}C, both γ-Mo_2N and δ-MoN phases, and also metallic Mo were present. Phase studies were extended to the molybdenum nitride films deposited from molybdenum hexacarbonyl $Mo(CO)_6$ and NH_3 between 350 and 700 ^{o}C.[159] The films deposited between 350 and 500 ^{o}C were polycrystalline and contained only the γ-Mo_2N phase. The films deposited at 550 ^{o}C and below 700 ^{o}C had a two-phase structure containing both δ-MoN and γ-Mo_2N phases. A single-phase δ-MoN film was obtained when the deposition temperature was 700 ^{o}C.

Table VII. Precursors, reaction temperatures, and properties of Mo-N CVD and ALD films.

Precursors	**Deposition temperature (°C)**	**Crystallinity**	**Properties**	**References**
CVD processes:				
$Mo(N(CH_3)_2)_4$-NH_3	200-400	amorphous	N/Mo ~ 1.4-1.5 H/Mo ~ 1.0 (200 °C) H/Mo ~ 0.45 (400 °C)	155,156
MoF_6-NH_3-H_2-Ar	500-700	MoN	not reported	157
$MoCl_5$-NH_3	400-800	Mo_2N, MoN, Mo	Cl not detected, C and O impurities	158,159
$Mo(CO)_6$-NH_3	350-700	Mo_2N, MoN	C and O impurities	159
ALD processes:				
$MoCl_5$-NH_3	400-500	Mo_2N, MoN	500 °C: 1 at% Cl, 100 μΩ cm 400 °C: 10 at% Cl	69,116
$MoCl_5$-Zn-NH_3	400-500	not reported	500 °C: < 1 at% Cl, 500 μΩ cm 400 °C: 7 at% Cl, 3 600 μΩ cm	69
$MoCl_5$-DMHy	400	Mo_2N, N rich matrix	3 at% Cl, 10 at% C, 2 at% O, 2 at% H, 930 μΩ cm	69

ALD of molybdenum nitride films has been only briefly described in the literature as can be seen in Table VII. In the first published study, molybdenum nitride films were deposited at 500 °C with $MoCl_5$ and NH_3 as precursors.[116] Both cubic γ-Mo_2N and hexagonal δ-MoN phases could be deposited, with resistivities of 260 and 250 μΩ cm, respectively. The same $MoCl_5$-NH_3 process was later studied by Juppo *et al.*[69] at 400 and 500 °C. The results obtained at 500 °C were fairly similar to those of earlier study,[116] as the deposited films had very low resistivity (100 μΩ cm) and chlorine content (1 at. %). However, the films deposited at 400 °C were of poor quality; the deposition rate was only 0.02 Å/cycle, the chlorine content was 10 at. %, and the sheet resistance could not be measured. The use of an additional Zn pulse ($MoCl_5$-Zn-NH_3) at 400 °C increased the deposition rate to 0.8 Å/cycle and decreased the Cl content to 7 at.

%, and the resistivity of the films was 3 600 μΩ cm. In the same study NH_3 was replaced with 1,1-dimethylhydrazine (DMHy). The films deposited at 400 ^oC with the $MoCl_5$-DMHy process had low resistivity (930 μΩ cm) and contained only 3 at. % chlorine. The films deposited with DMHy contained relatively large amounts of carbon, 10 at. %, but the contents of other impurities were less than 2 at. %.

3. Experimental

3.1. Film deposition

The film deposition experiments were carried out using a flow-type F-120 ALD reactor (ASM Microchemistry Ltd., Helsinki, Finland)[6] operated under a pressure of about 10 mbar. Nitrogen gas (purity 99.9995%) generated by a Nitrox UHPN 3000 nitrogen generator, was used for the transportation of the precursors and as a purging gas. The flow rate of nitrogen was 500 sccm (standard cubic centimeters per minute). Substrate materials were soda lime and borosilicate glasses and silicon, and the substrate size was 5 x 5 cm^2. The highest deposition temperature was 500 ^oC.

Solid precursors were evaporated from open boats held inside the reactor. All the liquid and gaseous precursors were held in external reservoirs. The external precursors were introduced to the reactor through needle and solenoid valves, and a mass flowmeter was used when necessary.

3.2. Film characterization

Film thicknesses (I,II,III,IV) and film composition (I) were determined with energy dispersive X-ray spectroscopy (EDX) using a Link ISIS EDX spectrometer installed to Zeiss DSM 962 scanning electron microscope (SEM) equipment. The EDX results were analyzed with a GMR Electron Probe Thin Film Microanalysis program[160] and converted to physical thicknesses using the bulk densities of TaN (16.3 g/cm^3)[13] and NbN (8.4 g/cm^3)[64]. The conformality was studied with the Zeiss DSM 962 SEM (I).

Film composition was determined by ion beam analysis using time-of-flight elastic recoil detection analysis (TOF-ERDA).[161,162] In TOF-ERDA, 53 MeV $^{127}I^{10+}$ ions or 18 MeV $^{63}Cu^{8+}$ ions (V), or 24 MeV $^{79}Br^{5+}$ ions (V) were utilized as a probing beam. Atomic concentrations of elements other than Ta were obtained from recoiled sample atoms, but scattered I^{10+} ions were used for Ta concentration (I,II,III). TOF-ERDA was also applied to obtain the deposition rates (V).

Crystallinity of the films was analyzed with a Philips MPD 1880 powder X-ray diffractometer (XRD) using Cu Kα radiation.

Sheet resistances were measured with the standard four-point probe method within 15 min after the film was exposed to air. Measurements were repeated after a few weeks to ensure that no significant changes had occurred. The resistivity values were calculated with use of the thicknesses determined by EDX analysis or TOF-ERDA (V).

For the diffusion barrier tests (I,IV,V), nitride films approximately 10 nm thick were deposited on silicon and covered with a Cu layer 100 nm thick deposited by an electron beam evaporator. The Cu/barrier/Si structures were annealed in nitrogen ambient at different temperatures. The thicknesses of the barrier films were determined by X-ray reflectance (XRR), and the copper silicide formation in the annealed films was determined by XRD in the grazing incidence mode, with an incidence angle of 1^{o} (I,IV,V). The XRR and XRD measurements were performed with a Bruker AXS D8 advance X-ray diffractometer using Cu Kα radiation. Also, sheet resistance measurements with the standard four-point probe method were used to determine the failure of the barrier (I,IV,V). The etch-pit method was applied to more sensitively determine the formation of copper silicide on the surface of the silicon substrate (IV,V). The samples were dipped into the Secco etch solution for 5 s (0.15 M K_2CrO_7/HF with ratio 1:2), which dissolved the formed copper silicides from the silicon substrate leaving pyramidal-shaped etch pits, which could be observed with SEM) (Fig. 5). The appearance of etch pits indicated the failure of the barrier layer. Before the samples could be Secco-etched, the Cu layer was selectively removed with a dilute HNO_3 solution and the nitride films were etched. The niobium nitride films (IV) were etched with a $NH_4OH/H_2O_2/H_2O$ solution with ratio 1:1:4, and the molybdenum nitride films (V) were etched with a $HCl/H_2O_2/H_2O$ solution with a ratio of 1:1:5.

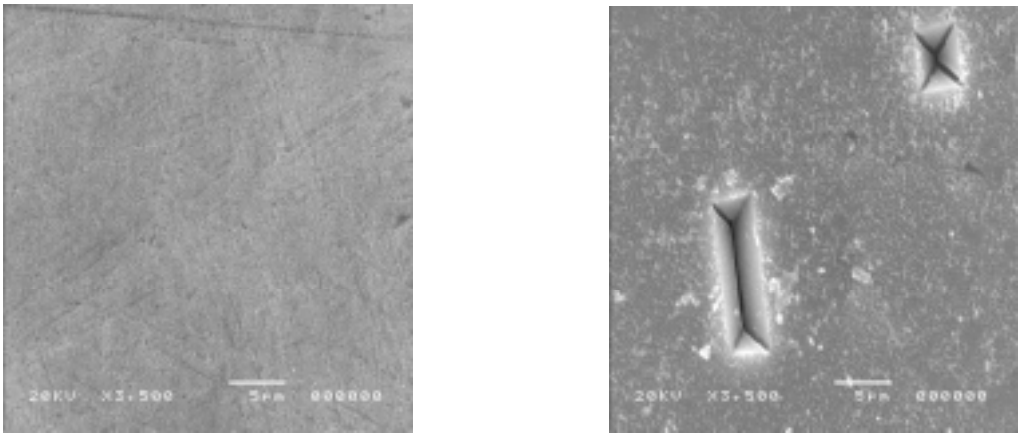

Figure 5. Two barrier samples after dipping into the Secco etch solution. The left picture is from an unfailed sample with a smooth surface and no etch pits. However, in the right picture two etch pits are clearly visible, indicating a failure.

Si/HfO_2/Ta(Si)N/TiN capacitors were prepared to carry out work function measurements on Ta(Si)N films (III). Ta(Si)N films about 50 nm thick were deposited at 400 and 500 ^oC on silicon substrates coated with ALD HfO_2 layers 3, 6, 9, and 15 nm thick. A 20-nm-thick TiN capping layer was deposited by sputtering on Ta(Si)N. Reactive ion etching (RIE) was used to pattern the gate electrodes to an area of 2.5 x 10^{-5} cm^2. The samples were annealed in forming gas (FGA) at 420 ^oC for 20 min, and the capacitance–voltage curves were measured at 1 MHz frequency. The NCSU CVC program[163] was used for the extraction of flat-band voltages (V_{FB}) and equivalent oxide thickness (EOT) of capacitors. The work function values were obtained by plotting V_{FB} as a function of EOT. The y-intercept of the plot gives the gate work function relative to the Fermi level of the Si substrate.

4. Results

This chapter summarizes the main results of the development of the ALD process for tantalum nitride, tantalum-silicon-nitride, niobium nitride, and molybdenum nitride films. Details can be found in the corresponding papers [I-V].

4.1. Trimethylaluminum as reducing agent for tantalum [I]

Ta(Al)N(C) films were deposited by ALD from $TaCl_5$ and NH_3 as precursors with use of trimethylaluminum (TMA) as an additional reducing agent for tantalum. The reducing ability of TMA is based on the relatively low dissociation energy of the Al–CH_3 bond (280 kJ/mol[164]). TMA decomposes to form •$Al(CH_3)_Z$ (Z=1,2) and •CH_3 radicals,[165] of which the •$Al(CH_3)_Z$ radical can react with the surface –$TaCl_x$ groups producing reduced tantalum and gaseous $Al(CH_3)_{3-X}Cl_X$. Although the decomposition of TMA contaminates the films with carbon and aluminum, the carbon contamination was not expected to destroy the barrier properties because titanium carbonitride films, among others, have shown good barrier properties.[166,167] Since TaC has relatively low resistivity,[123,168] the same was assumed to apply to tantalum carbonitrides. The aluminum incorporation, in turn, was expected to make the structure nanocrystalline or amorphous, and thereby improve the barrier properties.[91] TMA had already been used to deposit Ti(Al)N films by ALD.[169] The Ti(Al)N films had fairly low resistivity (140 μΩ cm at 400 °C) and moderately low chlorine content (< 4 at. % at 400 °C).

The objective of this work was to characterize the compositions, resistivities, and barrier properties of Ta(Al)N(C) films deposited at different temperatures. As a comparison, films were also deposited from $TaBr_5$ and NH_3 with and without an additional reducing agent. The reducing agents were Zn and TMA.

Film growth. In the study of film growth, first the process parameters were optimized, especially the length of the TMA pulse and its position in the deposition cycle. Variation of the TMA pulse length between 0.2 and 0.8 s in 0.3 s steps was found to have little influence on the film properties. On that basis, and because it appeared to saturate the growth rate well, 0.5 s was chosen as the TMA pulse length. Two pulsing schemes were examined in a study of the pulsing order: (i) $TaCl_5$-TMA-NH_3 and (ii) TMA-$TaCl_5$-NH_3. Since the films

deposited with the pulsing scheme (ii) contained more impurities, especially carbon, the pulsing scheme (i) was chosen for the following experiments. With the pulsing sequence $TaCl_5$-TMA-NH_3 (all pulse lengths 0.5 s), the deposition temperature was varied from 250 to 400 ^oC in steps of 50 ^oC. The highest deposition rate (0.94 Å/cycle) was obtained at 400 ^oC.

Film properties. The composition of the Ta(Al)N(C) films was strongly dependent on the deposition temperature. Both the chlorine and hydrogen (Fig. 6) contents decreased as the deposition temperature was increased. The film deposited at 250 ^oC contained as much as 14 at. % chlorine, whereas that deposited at 400 ^oC only 4 at. %. The carbon content of the films increased with the deposition temperature presumably because of the decomposition of TMA (Fig. 6). Similar temperature dependence of carbon incorporation had earlier been observed in ALD AlN films deposited from TMA and NH_3.[170] Even though the carbon content was fairly high in the film deposited at 400 ^oC (26 at. %), the carbon probably existed as carbide rather than hydrocarbon since the hydrogen content decreased with the increasing deposition temperature (Fig. 6). The aluminum content reached a maximum (12 at. %) at 350 ^oC. The oxygen content in the films was approximately 2 at. % at all deposition temperatures.

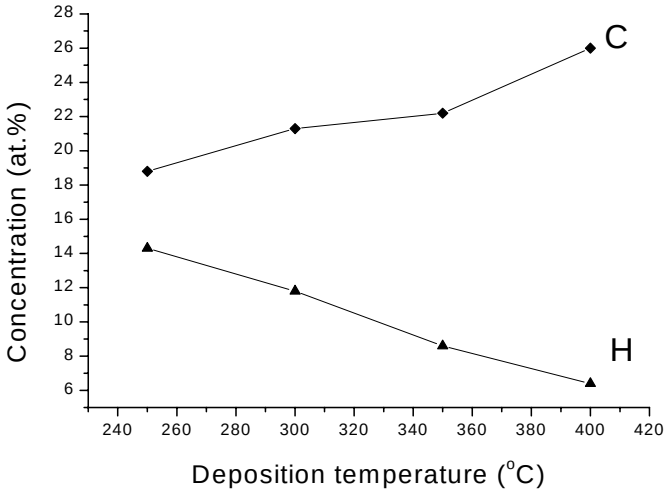

Figure 6. Carbon and hydrogen contents determined by TOF-ERDA of films deposited by the $TaCl_5$-TMA-NH_3 pulsing process as a function of deposition temperature.

The films were polycrystalline with cubic TaN structure. Films deposited at 300 °C and above were well crystallized. The lowest resistivity (1 300 μΩ cm) was obtained with the films deposited at 400 °C. Comparison of the resistivities agains the impurity contents suggests that chlorine is the most important impurity with respect to resistivity.

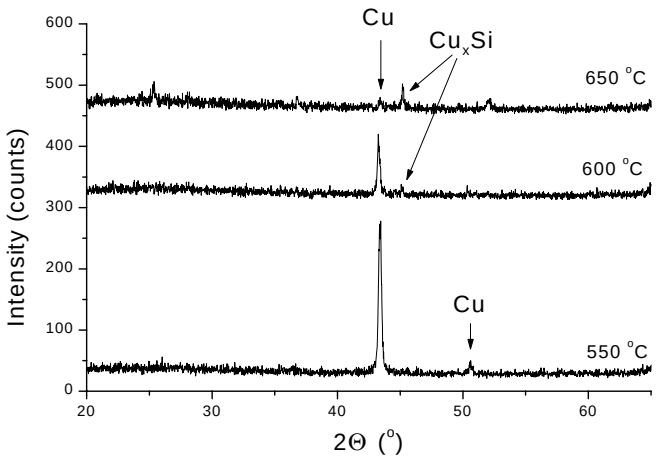

Figure 7. XRD patterns of Cu/Ta(Al)N(C)/Si structures annealed between 550 and 650 °C for 15 min in N_2 atmosphere.

As a means to studying the barrier properties, a 10-nm-thick Ta(Al)N(C) film was deposited on silicon and covered with copper to form a Cu/Ta(Al)N(C)/Si structure. The samples were annealed at temperatures between 400 and 700 °C in nitrogen ambient, and after that the sheet resistance was measured with the four-point probe, and the copper silicide formation was determined by XRD. The sheet resistance increased significantly after annealing at 650 °C and the copper silicide formation was observed after annealing at 600 °C (Fig. 7).

The films deposited with the pulsing sequence $TaBr_5$-TMA-NH_3 contained more impurities and had lower deposition rates and higher resistivities than the films deposited from $TaCl_5$. For comparison, films were also deposited with $TaBr_5$-NH_3 and $TaBr_5$-Zn-NH_3 sequences. The films deposited without zinc were most likely of the dielectric Ta_3N_5 phase, whereas the films deposited with zinc had the desired TaN phase.

In conclusion, TMA was an effective reducing agent. The films deposited from $TaCl_5$ and ammonia with use of TMA as a reducing agent had fairly low resistivity and were conductive TaN phase. Although the impurity contents were relatively high, the diffusion barrier tests indicated that the Cu/Ta(Al)N(C)/Si structure was stable against Cu diffusion up to 550 °C.

4.2. *tert*-Butylamine and allylamine as nitrogen sources and reducing agents for tantalum [II]

TaN films were deposited by ALD method from $TaCl_5$ and $TaBr_5$ with *tert*-butylamine ($^tBuNH_2$) or allylamine ($allylNH_2$) as reductive nitrogen source, with and without ammonia. The dissociation energy of ammonia is 453 kJ/mol,[171] whereas the dissociation energies of $^tBuNH_2$ and $allylNH_2$ are much lower, 346 and 290 kJ/mol, respectively.[172] The dissociation of the amines also gives rise to radicals, which may themselves reduce the tantalum precursor, or they may form new and even more reducing radicals. In the case of $^tBuNH_2$, first *tert*-butyl radicals are formed: $(CH_3)_3CNH_2 \rightarrow (CH_3)_3C\bullet + \bullet NH_2$. These may lead to the formation of atomic hydrogen: $(CH_3)_3C\bullet \rightarrow (CH_3)_2C{=}CH_2 + H\bullet$.[173] From this it was expected that $^tBuNH_2$ and $allylNH_2$ would be better reducing agents and nitrogen sources than ammonia.

The effect of the pulse lengths of $TaCl_5$ and $^tBuNH_2$ to the chlorine content, resistivity, and deposition rate were examined with the pulsing sequence $TaCl_5$-$^tBuNH_2$. Of the different pulse time combinations, the pulse lengths of 0.5 s for $TaCl_5$ and 1.0 s for $^tBuNH_2$ resulted in lowest chlorine content and resistivity. The same pulse length (0.5 s) was used for $TaBr_5$ as for $TaCl_5$. The flow rate for the two amines was 16 sccm.

A. Films deposited from $TaCl_5$ or $TaBr_5$ and $^tBuNH_2$

Film growth. The deposition rates obtained with the $TaCl_5$-$^tBuNH_2$ process varied between 0.25 and 0.35 Å/cycle. Those obtained with $TaBr_5$-$^tBuNH_2$ ranged only between 0.10 and 0.14 Å/cycle.

Film properties. With both processes, the amount of halogen impurities in the films deposited at 500 °C was less than 3 at. % (Fig 8). The films deposited at 500 °C contained 16-20 at. % carbon, compared to 1.8-3 at. % carbon in films

deposited at 400 °C (Fig 8). A similar trend in carbon content was earlier observed for ALD-deposited Ta(Al)N(C),[I] AlN,[170] and TiN[174] films. The oxygen contents in the films deposited from $TaCl_5$ were fairly low, varying between 2 and 6 at. %, whereas the films deposited from $TaBr_5$ contained considerably more oxygen (5-11 at. %). Hydrogen contents in films deposited from both tantalum precursors were below 2 at. %. The resistivities of the films showed strong temperature dependence: with both processes the resistivities of the films deposited at 500 °C were below 1 500 μΩ cm.

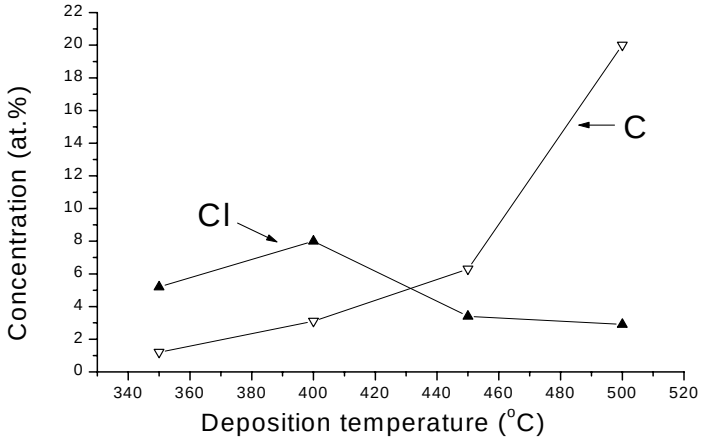

Figure 8. Carbon and chlorine contents of films deposited by the $TaCl_5$-^{t}$BuNH_2$ process as a function of the deposition temperature.

B. Films deposited from $TaCl_5$ or $TaBr_5$, NH_3, and ^{t}$BuNH_2$

Film growth. Three different pulsing sequences were used: TaX_5-^{t}$BuNH_2$-NH_3, TaX_5-NH_3-^{t}$BuNH_2$, and TaX_5-(^{t}$BuNH_2$+NH_3). The pulse length of the additional ammonia pulse was 0.5 s. In the last scheme, *tert*-butylamine and ammonia were pulsed at the same time and the pulse length was 1.0 s. The ammonia pulse was added to the pulsing sequence to see if it would decrease the carbon contamination and to ensure more complete formation of the TaN phase. The deposition rates varied between 0.23 and 0.30 Å/cycle for the tantalum chloride-based processes, but were as low as 0.06-0.14 Å/cycle for the tantalum bromide processes. These rates were similar to those obtained without ammonia.

Film properties. Of the three processes examined, the TaX_5-($^tBuNH_2$+NH_3) process gave the lowest chlorine and carbon contents. The chlorine content varied between 1 and 2 at. % (Fig. 9) and the bromide content between 1 and 3 at. %. The carbon content increased with the increasing deposition temperature in the films deposited with ammonia, but was consistently lower than in the films deposited without ammonia. The carbon content varied between 1.5 and 11 at. % with the tantalum chloride process (Fig 9), and between 0.6 and 7 at. % with the bromide process. In both cases the hydrogen contents were below 2 at. %. The oxygen content was higher in the films deposited from tantalum bromide: the film deposited at 450 °C from tantalum bromide contained 10 at. % oxygen, while the film deposited from tantalum chloride at the same temperature contained 5 at. % oxygen.

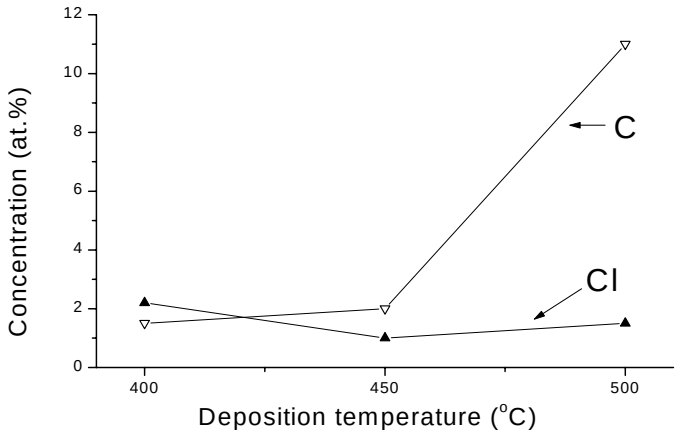

Figure 9. Carbon and chlorine contents of the films deposited by the $TaCl_5$–($^tBuNH_2$+NH_3) process as a function of deposition temperature.

The resistivities obtained with tantalum chloride were lower than those obtained with tantalum bromide most likely because of the lower oxygen content of the films. The resistivities of the films deposited at 500 °C with the TaX_5-($^tBuNH_2$+NH_3) process were 1 900 μΩ cm for tantalum chloride and 2 700 μΩ cm for tantalum bromide.

C. Films deposited from $TaCl_5$ and allylNH_2 with and without NH_3

Using allylamine as a reducing agent, five pulsing sequences were examined at 400 °C: $TaCl_5$-allylNH_2, $TaCl_5$-allylNH_2-NH_3, $TaCl_5$-(allylNH_2+NH_3), $TaCl_5$-(allylNH_2+NH_3)-NH_3, and $TaCl_5$-NH_3-(allylNH_2+NH_3). The pulse length of the allylamine was 0.5 s and this same duration was used when allylamine and ammonia were pulsed at the same time. The deposition rate varied between 0.19 and 0.23 Å/cycle. The films contained large amounts of impurities, especially chlorine, and the resistivities were higher than those obtained with *tert*-butylamine. The lowest resistivity (18 000 μΩ cm at 400 °C) was obtained with the $TaCl_5$-(allylNH_2+NH_3) process.

It can be concluded that both *tert*-butylamine and allylamine are able to act as reducing agents for tantalum halides, and the desired TaN phase is obtained. The films deposited with *tert*-butylamine had lower resistivities and chlorine contents than those deposited with allylamine. In the both cases the addition of ammonia to the process lowered carbon contents. In general, the results obtained with tantalum chloride were better than those obtained with tantalum bromide.

4.3. Tris(dimethylamino)silane as silicon precursor and reducing agent for tantalum [III]

Ta(Si)N films were deposited from $TaCl_5$ and ammonia with use of tris(dimethylamino)silane ($(CH_3)_2N)_3SiH$, TDMAS) as additional reducing agent and a silicon precursor. TDMAS was chosen as silicon precursor because, although it is a silane derivative with a Si-H bond, it is easier to handle and less toxic than SiH_4 or Si_2H_6. In addition, there are no direct silicon–carbon bonds in TDMAS and minimal incorporation of carbon impurities into the films was expected. On the other hand, as TDMAS had earlier been used in CVD of silicon nitride[175-178] and silicon oxynitride[179] films, the formation of nonconductive silicon nitride phase was considered possible and a potential drawback. Another possible side-reaction could lead to the formation of $TaSi_x$. In separate experiments, however, no films were deposited by alternate supply of TDMAS and either $TaCl_5$ or NH_3.

Film growth. First different pulsing sequences were examined with and without additional ammonia pulses. Five pulsing sequences were studied at 400 °C:

$TaCl_5$-TDMAS-NH_3, $TaCl_5$-NH_3-TDMAS-NH_3, $TaCl_5$-(TDMAS+NH_3), $TaCl_5$-(TDMAS+NH_3)-NH_3, and $TaCl_5$-NH_3-(TDMAS+NH_3) (Table VIII). In the three last pulsing sequences, TDMAS and NH_3 were pulsed into the reactor at the same time. As no improvement in was observed with the additional ammonia pulses the $TaCl_5$-TDMAS-NH_3 pulsing sequence was chosen for further experiments. The pulse length of TDMAS was then optimized. Reasonably high deposition rate was obtained with the pulse length of 1.0 s. In experiments investigating the effect of the deposition temperature with the pulsing sequence $TaCl_5$-TDMAS-NH_3 and pulse lengths 0.5, 1.0, and 0.5 s the deposition rate varied between 0.23 and 0.34 Å/cycle. The highest deposition rate was obtained at 500 ^oC.

Table VIII. Deposition sequences and the obtained resistivities and deposition rates.

Sequence	**Pulsing order**	**Pulse lengths (s)**	**Resistivity (μΩ cm)**	**Dep. rate (Å/cycle)**
1.	$TaCl_5$-TDMAS-NH_3	0.5, 1.0, 0.5	36 000	0.32
2.	$TaCl_5$-(TDMAS+NH_3)	0.5, 1.0	37 000	0.34
3.	$TaCl_5$-NH_3-TDMAS-NH_3	0.5, 0.5,1.0, 0.5	79 000	0.40
4.	$TaCl_5$-(TDMAS+NH_3)-NH_3	0.5, 1.0, 0.5	220 000	0.40
5	$TaCl_5$-NH_3-(TDMAS+NH_3)	0.5, 0.5, 1.0	200 000	0.31

Film properties. The chlorine content showed strong temperature dependence. The film deposited at 300 ^oC contained as much as 10 at. % chlorine, whereas the films deposited at 450 and 500 ^oC contained less than 1 at. % chlorine (Fig. 10). In all films the hydrogen and carbon contents were low. The oxygen content varied between 3 and 5 at. %. The silicon content was highest (8 at. %) in the film deposited at 500 ^oC (Fig. 10). Since the films deposited at 300 and 350 ^oC were partly transparent, yellowish, and amorphous, it is highly probable that they were dielectric Ta_3N_5 phase. The films deposited above 350 ^oC showed typical XRD reflections of the cubic TaN. Those deposited between 450 and 500 ^oC had resistivities below 10 000 μΩ cm.

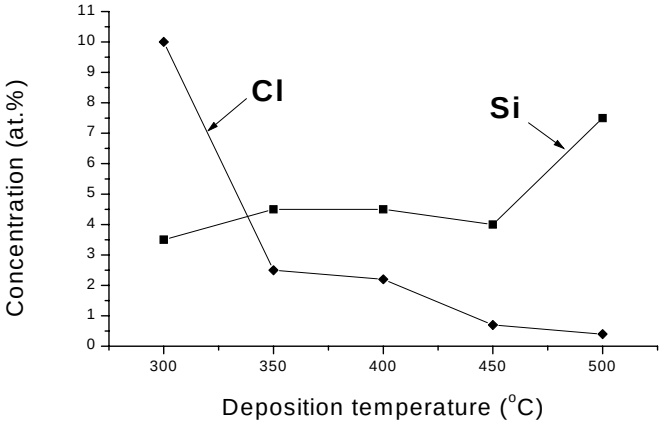

Figure 10. Chlorine and silicon contents of the Ta(Si)N films as a function of deposition temperature.

Si/HfO_2/Ta(Si)N/TiN capacitors with different HfO_2 thicknesses were prepared to evaluate the work function values of the Ta(Si)N films. Two temperatures, 400 and 500 °C, were used for the film deposition. The work functions of the samples annealed under forming gas were not significantly different for the two deposition temperatures: 4.8 eV for 400 °C and 4.7 eV for 500 °C.

By way of summary, the Ta(Si)N films deposited at 450 and 500 °C contained very few impurities, less than 1 at. % each of chlorine, carbon and hydrogen. The resistivities of the films were considerably higher than for the previously examined (I,II) ALD TaN films. The high values are likely due to the incorporation of nonconductive silicon nitride. The work function values of the Ta(Si)N films deposited at 400 and 500 °C were more mid-gap-like rather than the expected n-type.

4.4. $NbCl_5$ and NH_3 [IV]

NbN_x films were deposited with use of $NbCl_5$ and NH_3 as precursors. In contrast to the earlier studies with high deposition temperatures,[65,66,69,116] also low deposition temperatures, down to 250 °C, were explored. The barrier properties of NbN_x films deposited at 350, 400, and 500 °C were studied and compared with those of Nb(Ta)N and Nb(Ti)N films deposited at 400 °C.

Film growth. The deposition rate increased with deposition temperature increasing from 250 to 500 °C. The highest deposition rate, 0.27 Å/cycle, was obtained at 500 °C. When the deposition temperatures were 300 and 400 °C, the deposition rates were 0.16 and 0.17 Å/cycle, respectively.

Film properties. All the NbN_x films had a metallic and mirror-like appearance. The film deposited at 500 °C was almost chlorine-free, whereas that deposited at 250 °C contained as much as 8 at. % chlorine (Fig. 11). The films deposited at 300 and 400 °C contained 6 and 1 at. % chlorine, respectively. The oxygen content was approximately 1 at. % in all films regardless of the deposition temperature. The Nb/N ratio was more or less the same at all deposition temperatures, being close to 0.8 (Fig. 11).

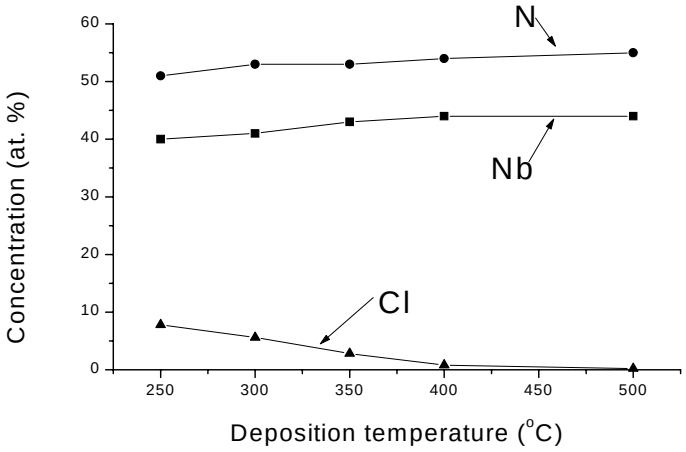

Figure 11. Niobium, nitrogen, and chlorine contents of the NbN_x films deposited at different temperatures.

XRD measurements showed that the NbN_x films were polycrystalline, except the film deposited at 250 °C. The films deposited between 300 and 500 °C showed reflections with d-values that match very well with the reference values of tetragonal Nb_4N_5: 2.503, 2.166, and 1.531 Å corresponding to the (211), (301)/(002), and (402)/(312) reflections, respectively.[180] Likewise, the Nb/N ratio (Fig. 11) supports the existence of the Nb_4N_5 phase. The resistivities of the NbN_x films showed strong temperature dependence. The resistivity of the film

deposited at 250 °C was approximately 16 000 μΩ cm, whereas that of the film deposited at 500 °C was only 600 μΩ cm.

Barrier characteristics. The barrier properties were studied for NbN_x films deposited at 350, 400, and 500 °C (Table IX). A third element (Ta or Ti) was added to the NbN_x films deposited at 400 °C, and the barrier capabilities of these ternary nitrides (Nb(Ta)N and Nb(Ti)N) were investigated by way of comparison. The test structures were formed by depositing the barrier films on silicon substrates and covering them with a layer of copper 100 nm thick. The samples were then annealed in nitrogen ambient for 15 min at temperatures from 450 to 700 °C with intervals of 50 °C. The sheet resistance and XRD data were measured from the annealed samples Etch pit-tests were performed after the selective etching of copper and nitride films.

Table IX. Niobium nitride films studied in the barrier tests, their accurate thicknesses, and the breakdown temperatures found by the different testing methods.

Structure	Deposition temperature (°C)	Thickness determined by XRR (nm)	$T_{breakdown}$ R_s (°C)	$T_{breakdown}$ XRD (°C)	$T_{breakdown}$ etch-pit (°C)
NbN_x	350	10.9	700	500	500
NbN_x	400	10.3	700	600	600
NbN_x	500	9.9	700	600	600
Nb(Ta)N	400	10.3	700	600	600
Nb(Ti)N	400	12.5	700	600	600

The results that were obtained were very good (see sect. 2.3.3) considering the thickness and low deposition temperatures of the barriers. A comparison of the breakdown temperatures of the NbN_x films with those of Nb(Ta)N and Nb(Ti)N films reveals no improvement upon the addition of tantalum or titanium to the films.

4.5. $MoCl_5$ and NH_3 [V]

Molybdenum nitride films were deposited from $MoCl_5$ and NH_3 with no additional reducing agent in a temperature range of 350 to 500 °C. The properties of ALD molybdenum nitride films had earlier been only briefly described.[69,116] The main focus was to study the deposition of MoN_x films at low temperatures and determine their barrier properties. The barrier tests were performed with MoN_x films approximately 10 nm thick deposited at 350, 400, and 500 °C. For comparison, the barrier properties of Mo(Ta)N and Mo(Ti)N films deposited at 400 °C were examined.

Film growth. The deposition rate first increased as a function of the deposition temperature from 0.23 (350 °C) to 0.38 Å/cycle (450 °C) but then dropped to just 0.22 Å/cycle at 500 °C (Fig. 12). The low deposition rate at 500 °C is assumed to be due to an etching reaction. The same kind of etching reaction was observed when metallic molybdenum was deposited by ALD with use of $MoCl_5$ and Zn as precursors.[181]

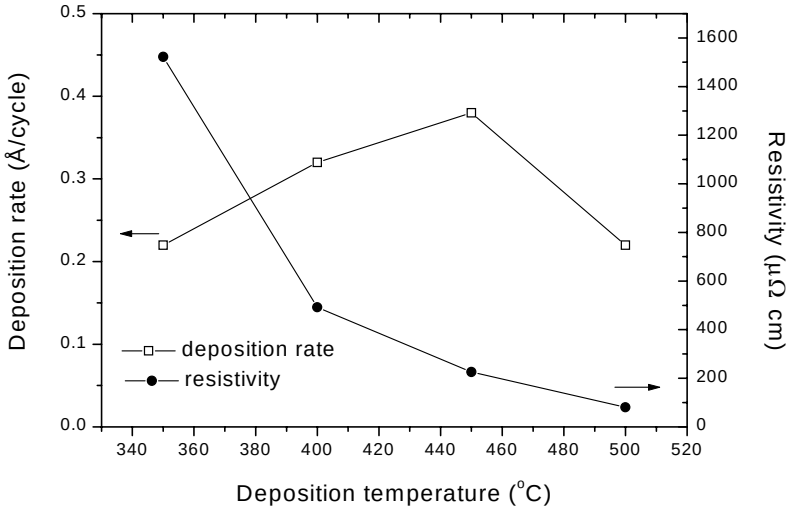

Figure 12. Deposition rates and resistivities of the MoN_x films as a function of deposition temperature.

Film properties. The metallic and mirror-like MoN_x films contained less than 0.3 at. % chlorine when deposited at and above 400 °C. The films were fairly free from impurities; the oxygen and hydrogen contents were less than 1.5 and 0.6 at. %, respectively. The Mo:N ratio changed from 1:1.2 (350 °C) to 1:1.1 (500 °C). XRD measurements showed that the films were polycrystalline. The film deposited at 350 °C showed peaks corresponding to the γ-Mo_2N phase.[182] The films deposited at 400 and 450 °C contained both MoN[183] and γ-Mo_2N phases, whereas the film deposited at 500 °C consisted of the MoN phase alone. According to TOF-ERDA, however, the film compositions were $MoN_{1.2}$ at 350 °C and $MoN_{1.1}$ at 500 °C, indicating the presence of nitrogen-rich amorphous phase especially at low deposition temperatures. The resistivity was strongly dependent on the deposition temperature, being less than 100 μΩ cm in the film deposited at 500 °C (Fig. 12).

Barrier characteristics. The diffusion barrier characteristics of MoN_x were studied for films deposited on silicon at 350, 400, and 500 °C and covered with a Cu layer approximately 100 nm thick (Table X). The addition of TaN_x or TiN, with deposition at 400 °C, to MoN_x was examined to see if it could enhance the barrier properties relative to pure MoN_x. The capability of the barrier layer to prevent the interdiffusion of Cu and Si was studied for annealed samples by measuring sheet resistance values and analyzing XRD data. The etch-pit method was used to sensitively determine the formation of copper silicide on the surface of silicon substrate.

Table X. Molybdenum nitride films studied in the barrier tests, their accurate thicknesses, and the breakdown temperatures found by different testing methods.

Structure	Deposition temperature (°C)	Thickness determined by XRR (nm)	$T_{breakdown}$ R_s (°C)	$T_{breakdown}$ XRD (°C)	$T_{breakdown}$ Secco (°C)
MoN_x	350	11.0	700	600	600
MoN_x	400	10.7	> 700	650	650
MoN_x	500	11.1	> 700	> 700	650
Mo(Ta)N	400	9.4	650	650	600
Mo(Ti)N	400	8.7	> 700	650	600

The breakdown temperatures obtained for molybdenum nitride barriers were reasonably high relative to those obtained for other ALD deposited barrier materials (see sect. 2.3.3 and publication V). The MoN_x barriers deposited at 400 and 500 ^oC failed only after annealing at 650 ^oC, when the first etch pits were observed. The addition of Ta or Ti did not effect any improvement in the barrier properties of MoN_x deposited at 400 ^oC, as the Mo(Ta)N and Mo(Ti)N barriers were less stable than the MoN_x barrier.

5. Conclusions

The rapidly shrinking device size that will characterize future integrated circuitry generations creates a variety of new challenges. There is great need for a deposition technique that produces films with good material properties, excellent conformality in high aspect ratio structures, and large area uniformity at low deposition temperatures. One of the most promising techniques in this respect is atomic layer deposition (ALD). It is highly likely that ALD processes will be used in the device fabrication in the next few years.[2,184,185,186] Ultrathin diffusion barrier layers for copper interconnects will be among the first ALD applications.

The requirements for barrier materials are tough. They need to be electrically conductive, thermodynamically stable and unreactive with materials above and below, and the microstructure should be amorphous or nanocrystalline. Transition metal nitrides, metal silicides, and metal-silicon-nitrides are considered the most promising candidates when it comes to providing the required physical, chemical, and electrical properties. The present study on the atomic layer deposition of tantalum, niobium, and molybdenum nitrides was a contribution to this search for improved barrier materials.

The main difficulty in the deposition of tantalum nitride films is the lack of suitable reducing agents. Usually, tantalum exists in a precursor in oxidation state +V and obtaining the desired cubic TaN phase requires an effective reducing agent. In this study, tantalum nitride films were deposited with four different reducing agents.

The films deposited with TMA as additional reducing agent [I] showed relatively low resistivities: the lowest resistivity was 1 300 μΩ cm at 400 ^{o}C. All films contained considerable amounts of aluminum and carbon impurities. In the barrier tests, a Ta(Al)N(C) film 10 nm thick remained stable against Cu diffusion up to 550 ^{o}C. The films deposited with ^{t}BuNH$_2$ contained only minor amounts of impurities when an additional NH_3 pulse was used, and the films were conductive TaN phase already at 400 ^{o}C [II]. The resistivities were higher than those obtained with TMA [I], however. The results obtained with allylNH$_2$ were not as good as those obtained with ^{t}BuNH$_2$ [II]. When TDMAS was used as an extra reducing agent in the deposition of Ta(Si)N films [III], the films deposited at and above 450 ^{o}C were almost free of impurities, but the resistivities were

fairly high. A potential new application for tantalum nitride and tantalum-silicon-nitrides is as gate metal replacing the polycrystalline silicon electrode. The work function values of the Ta(Si)N films deposited at 400 and 500 ^{o}C and annealed in forming gas were 4.8 and 4.7 eV, respectively.

Niobium nitride and molybdenum nitride films were deposited from the corresponding metal chlorides ($NbCl_5$ and $MoCl_5$) and ammonia without an additional reducing agent. The ALD method had been used to deposit NbN_x and MoN_x films earlier but mostly at as high a temperature as 500 ^{o}C. A goal of this work was to lower the deposition temperature, while at the same time improving film properties, especially diffusion barrier properties. In this study, NbN_x films were deposited over a broad temperature range from 250 to 500 ^{o}C [IV]. Films deposited at 400 and 500 ^{o}C had resistivity below 750 μΩ cm. The approximately 10-nm-thick NbN_x films deposited at 400 and 500 ^{o}C showed thermal integrity up to 550 ^{o}C. MoN_x films were deposited at temperatures from 350 to 500 ^{o}C [V]. These films exhibited somewhat lower resistivities than those of the NbN_x films–below 500 μΩ cm for films deposited at and above 400 ^{o}C. Furthermore, the MoN_x barriers deposited at 400 and 500 ^{o}C showed superior diffusion barrier properties: no etch pits could be observed after the annealing at 600 ^{o}C.

The results of this study are promising. Four new reducing agents were succesfully applied in the deposition of the conductive TaN films, and NbN_x and MoN_x films with attractive properties were deposited at relatively low temperatures. The films reported in publications I-V show promise for applications in many areas, and most interestingly, microelectronic devices.

References

1. G.E. Moore, Cramming more components onto integrated circuits, *Electronics* 38 (1965) 114-117.
2. *International Technology Roadmap for Semiconductors* (Semiconductor Industry Association, San Jose, CA, 2001).
3. A.E. Kaloyeros and E. Eisenbraun, *Annu. Rev. Mater. Sci.* 30 (2000) 363-385.
4. Y.-S. Suh, G. Heuss, H.Z. Zhong, S.-N. Hong, and V. Misra, *VLSI Tech. Dig.* (2001) 47-48.
5. T. Suntola, J. Antson, A. Pakkala, and S. Lindfors, *SID 80 Dig.* 11 (1980) 109.
6. T. Suntola, *Thin Solid Films* 216 (1992) 84-89.
7. M. Ritala and M. Leskelä, *Nanotechnology* 10 (1999) 19-24.
8. *Encyclopedia of Inorganic Chemistry*, Ed. R.B. King, John Wiley & Sons Ltd., Chichester, 1994, Vol. 5, p. 2498.
9. N. Terao, *Jpn. J. Appl. Phys.* 10 (1971) 249-259.
10. C.-S. Shin, Y.-W. Kim, D. Gall, J.E. Greene, and I. Petrov, *Thin Solid Films* 402 (2002) 172-182.
11. A.Y. Ganin, L. Kienle, and G.V. Vajenine, *Eur. J. Inorg. Chem.* (2004) 3233-3239.
12. *Encyclopedia of Inorganic Chemistry*, Ed. R.B. King, John Wiley & Sons Ltd., Chichester, 1994, Vol. 5, p. 2508.
13. *CRC Handbook of Chemistry and Physics*, 82 nd ed., Ed. D.R. Lide, CRC Press LLC, 2001-2002, p. 4-88.
14. K.-H. Min, K.-C. Chun, and K.-B. Kim, *J. Vac. Sci. Technol.* B 14 (1996) 3263-3269.
15. T. Laurila, K. Zeng, J.K. Kivilahti, J. Molarius, T. Riekkinen, and I. Suni, *Microelectronic Eng.* 60 (2002) 71-80.
16. Z.-C. Wu, C.-C. Wang, R.-G. Wu, Y.-L. Liu, P.-S. Chen, Z.-M. Zhu, M.-C. Chen, J.-F. Chen, C.-I. Chang, and L.-J. Chen, *J. Electrochem. Soc.* 146 (1999) 4290-4297.
17. A.E. Kaloyeros, X. Chen, T. Stark, K. Kumar, S.-C. Seo, G.G. Peterson, H.L. Frisch, B. Arkles, and J. Sullivan, *J. Electrochem. Soc.* 146 (1999) 170-176.
18. S.-L. Cho, K.-B. Kim, S.-H. Min, H.-K. Shin, and S.-D. Kim, *J. Electrochem. Soc.* 146 (1999) 3724-3730.

19. S.J. Im, S.-H. Kim, K.-C. Park, S.-L. Cho, and K.-B. Kim, *Mat. Res. Soc. Symp. Proc.* 612 (2000) D6.7.1-D6.7.6.
20. D. Fischer, T. Scherg, J.G. Bauer, H.-J. Schulze, and C. Wenzel, *Microelectronic Eng.* 50 (2000) 459-464.
21. C.-L. Lin, S.-R. Ku, and M.-C. Chen, *Jpn. J. Appl. Phys.* 40 (2001) 4181-4186.
22. H.-J. Bae, Y.-H. Shin, and C. Lee, *J. Kor. Phys. Soc.* 34 (1999) 504-509.
23. C. Lee and Y.-H. Shin, *Mat. Chem. Phys.* 57 (1998) 17-22.
24. Y.-J. Lee, B.-S. Suh, S.-K. Rha, and C.-O. Park, *Thin Solid Films* 320 (1998) 141-146.
25. S. Gopalan, K. Onishi, R. Nieh, C.S. Kang, R. Choi, H.-J. Cho, S. Krishnan, and J.C. Lee, *Appl. Phys. Lett.* 80 (2002) 4416-4418.
26. J.K. Schaeffer, S.B. Samavedam, D.C. Gilmer, V. Dhandapani, P.J. Tobin, J. Mogab, B.-Y. Nguyen, B.E. White, Jr., S. Dakshina-Murthy, R.S. Rai, Z.-X. Jiang, R. Martin, M.V. Raymond, M. Zavala, L.B. La, J.A. Smith. R. Garcia, D. Roan, M. Kottke, and R.B. Gregory, *J. Vac. Sci. Technol.* B 21 (2003) 11-17.
27. Y.-S. Suh, G.P. Heuss, and V. Misra, *Appl. Phys. Lett.* 80 (2002) 1403-1405.
28. Y.-S. Suh, G.P. Heuss, V. Misra, D.-G. Park, and K.-Y. Lim, *J. Electrochem. Soc.* 150 (2003) F79-F82.
29. C. Chaneliere, J.L. Autran, R.A.B. Devine, and B. Balland, *Mater. Sci. Eng. Rep.* R22 (1998) 269-322.
30. J.-C. Chuang and M.-C. Chen, *J. Electrochem. Soc.* 145 (1998) 3170-3177.
31. C. Cabral, Jr., K.L. Saenger, D.E. Kotecki, and J.M.E. Harper, *J. Mater. Res.* 15 (2000) 194-198.
32. T. Yeh, D. Swanson, L. Berg, and P. Karn, *IEEE Trans. Magn.* 33 (1997) 3631-3633.
33. I. Ayerdi, E. Castaño, A. García-Alonso, and J. Gracia, *Sens. Actuators* A 60 (1997) 72-75.
34. C. Linder, A. Dommann, G. Staufert, and M.-A. Nicolet, *Sens. Actuators* A 61 (1997) 387-391.
35. Y.X. Leng, H. Sun, P. Yang, J.Y. Chen, J. Wang, G.J. Wan, N. Huang, X.B. Tian, L.P. Wang, and P.K. Chu, *Thin Solid Films* 398-399 (2001) 471-475.

36. *Encyclopedia of Inorganic Chemistry*, Ed. R.B. King, John Wiley & Sons Ltd., Chichester, 1994, Vol. 5, p. 2504, 2507.
37. G. Brauer and W. Kern, *Z. Anorg. Allg. Chem*. 507 (1983) 127-141.
38. W. Lengauer, M. Bohn, B. Wollein, and K. Lisak, *Acta Mater.* 48 (2000) 2633-2638.
39. R.E. Treece, J.S. Horwitz, S.B. Qadri, E.F. Skelton, E.P. Donovan, and D.B. Chrisey, *J. Solid State Chem.* 117 (1995) 294-299.
40. Y.M. Shy, L.E. Toth, and R. Somasundaram, *J. Appl. Phys.* 44 (1973) 5539-5545.
41. T. Ishiguro, K. Matsushima, and K. Hamasaki, *J. Appl. Phys.* 73 (1993) 1151-1153.
42. R.E. Treece, J.S. Horwitz, J.H. Claassen, and D.B. Chrisey, *Appl. Phys. Lett.* 65 (1994) 2860-2862.
43. A.B. Kaul, T.D. Sands, and T. Van Duzer, *J. Mater. Res.* 16 (2001) 1223-1226.
44. *CVD of Nonmetals*, Ed. W.S. Rees, Jr., VCH Verlagsgesellschaft GmbH, Weinheim, 1996, p. 62.
45. *CRC Handbook of Chemistry and Physics*, 82nd ed., Ed. D.R. Lide, CRC Press LLC, 2001-2002, p.12-85.
46. W. Mayr, W. Lengauer, V. Buscaglia, J. Bauer, M. Bohn, and M. Fialin, *J. Alloys Compd.* 262-263 (1997) 521-528.
47. Z. Wang, A. Kawakami, Y. Uzawa, and B. Komiyama, *J. Appl. Phys.* 79 (1996) 7837-7842.
48. Z. Wang, H. Terai, A. Kawakami, and Y. Uzawa, *Appl. Phys. Lett.* 75 (1999) 701-703.
49. J. Zhang, N. Boiadjieva, G. Chulkova, H. Deslandes, G.N. Goltsman, A. Korneev, P. Kouminov, M. Leibowitz, W. Lo, R. Malinsky, O. Okunev, A. Pearlman, W. Slysz, K. Smirnov, C. Tsao, A. Verevkin, B. Voronov, K. Wilsher, and R. Sobolewski, *Electron. Lett.* 39 (2003) 1086-1088.
50. G. Goltsman, A. Korneev, V. Izbenko, K. Smirnov, P. Kouminov, B. Voronov, N. Kaurova, A. Verevkin, J. Zhang, A. Pearlman, W. Slysz, and R. Sobolewski, *Nucl. Instrum. Methods Phys. Res*. Sect. A 520 (2004) 527-529.
51. B. Delaet, J.-C. Villegier, W. Escoffier, J.-L. Thomassin, P. Feautrier, I. Wang, P. Renaud-Goud, and J.-P. Poizat, *Nucl. Instrum. Methods Phys. Res.* Sect. A 520 (2004) 541-543.

52. K.S. Havey, J.S. Zabinski, and S.D. Walck, *Thin Solid Films* 303 (1997) 238-245.
53. F. Lévy, P. Hones, P.E. Schmid, R. Sanjinés, M. Diserens, and C. Wiemer, *Surf. Coat. Technol.* 120-121 (1999) 284-290.
54. M. Benkahoul, E. Martinez, A. Karimi, R. Sanjinés, and F. Lévy, *Surf. Coat. Technol.* 180-181 (2004) 178-183.
55. V.N. Zhitomirsky, I. Grimberg, L. Rapoport, N.A. Travitzky, R.L. Boxman, S. Goldsmith, and B.Z. Weiss, *Surf. Coat. Technol.* 120-121 (1999) 219-225.
56. L. Hultman, C. Engström, and M. Odén, *Surf. Coat. Technol.* 133-134 (2000) 227-233.
57. Y. Long, R.J. Stearn, Z.H. Barber, S.J. Lloyd, and W.J. Clegg, *Mat. Res. Soc. Symp. Proc.* 791 (2004) Q5.18.1-Q5.18.6.
58. J.J. Jeong and C.M. Lee, *Appl. Surf. Sci.* 214 (2003) 11-19.
59. A. Madan, S.A. Barnett, A. Misra, H. Kung, and M. Nastasi, *J. Vac. Sci. Technol.* A 19 (2001) 952-957.
60. X. Yu, Q. Lai, G. Li, J. Xu, and M. Gu, *J. Mat. Sci. Lett.* 21 (2002) 1671-1673.
61. M. Fenker, M. Balzer, R.V. Büchi, H.A. Jehn, H. Kappl, ad J.-J. Lee, *Surf. Coat. Technol.* 163-164 (2003) 169-175.
62. Y. Gotoh, M. Nagao, T. Ura, H. Tsuji, and J. Ishikawa, *Nucl. Instrum. Methods Phys. Res.* Sect. B 148 (1999) 925-929.
63. Y. Gotoh, H. Tsuji, and J. Ishikawa, *Rew. Sci. Instrum.* 71 (2000) 1002-1005.
64. *CRC Handbook of Chemistry and Physics*, 82nd ed., D.R. Lide, Editor, CRC Press LLC, 2001-2002, p. 4-72.
65. K.-E. Elers, M. Ritala, M. Leskelä, and E. Rauhala, *Appl. Surf. Sci.* 82/83 (1994) 468-474.
66. M. Ritala, T. Asikainen, M. Leskelä, J. Jokinen, R. Lappalainen, M. Utriainen, L. Niinistö, and E. Ristolainen, *Appl. Surf. Sci.* 120 (1997) 199-212.
67. M. Nagai, R. Nakauchi, Y. Ono, and S. Omi, *Catal. Today* 57 (2000) 297-304.
68. *CRC Handbook of Chemistry and Physics*, 82 nd ed., Ed. D.R. Lide, CRC Press LLC, 2001-2002, p.4-70.
69. M. Juppo, M. Ritala, and M. Leskelä, *J. Electrochem. Soc.* 147 (2000) 3377-3381.

70. C.L. Bull, P.F. McMillan, E. Soignard, and K. Leinenweber, *J. Solid State Chem.* 177 (2004) 1488-1492.
71. E. Furimsky, *Appl. Catal. A: Gen.* 240 (2003) 1-28.
72. P. Liu and J.A. Rodriguez, *Catal. Lett.* 91 (2003) 247-252.
73. T. Kadono, T. Kubota, and Y. Okamoto, *Catal. Today* 87 (2003) 107-115.
74. S. Gong, H. Chen, W. Li, and B. Li, *Catal. Commun.* 5 (2004) 621-624.
75. M. Nagai, Y. Yamamoto, and R. Aono, *Colloids Surf. A: Physicochem. Eng. Aspects* 241 (2004) 257-263.
76. Y. Li, Y. Fan, J. He, B. Xu, H. Yang, J. Miao, and Y. Chen, *Chem. Eng. J.* 99 (2004) 213-218.
77. R. Kojima and K. Aika, *Appl. Catal. A: Gen.* 219 (2001) 141-147.
78. H.J. Lee, J.-G. Choi, C.W. Colling, M.S. Mudholkar, and L.T. Thompson, *Appl. Surf. Sci.* 89 (1995) 121-130.
79. X. Chen, T. Zhang, M. Zheng, Z. Wu, W. Wu, and C. Li, *J. Catal.* 224 (2004) 473-478.
80. E. Soignard, P.F. McMillan, T.D. Chaplin, S.M. Farag, C.L. Bull, M.S. Somayazulu, and K. Leinenweber, *Phys. Rew. B* 68 (2003) 132101-1–132101-4.
81. J.E. Lowther, *J. Alloys Compd.* 364 (2004) 13-16.
82. R. Sanjinés, P. Hones, and F. Lévy, *Thin Solid Films* 332 (1998) 225-229.
83. P. Hones, N. Martin, M. Regula, and F. Lévy, *J. Phys. D: Appl. Phys.* 36 (2003) 1023-1029.
84. C. Wiemer, R. Sanjinés, and F. Lévy, *Surf. Coat. Technol.* 86-87 (1996) 372-376.
85. J. Kozlowski, J. Markowski, A. Prajzner, and J. Zdanowski, *Surf. Coat. Technol.* 98 (1998) 1440-1443.
86. H. Kung, T.R. Jervis, J.-P. Hirvonen, T.E. Mitchell, and M. Nastasi, *Nanostruct. Mater.* 7 (1996) 81-88.
87. J.-Y. Lee and J.-W. Park, *Jpn. J. Appl. Phys.* 35 (1996) 4280-4284.
88. J.-C. Chuang, S.-L. Tu, and M.-C. Chen, *Thin Solid Films* 346 (1999) 299-306.
89. Y. He and J.Y. Feng, *J. Cryst. Growth* 263 (2004) 203-207.
90. S. Haukka, K.-E. Elers, and M. Tuominen, *Mat. Res. Soc. Symp. Proc.* 612 (2001) D6.4/1-D6.4/6.
91. C.E. Ramberg, E. Blanquet, M. Pons, C. Bernard, and R. Madar, *Microelectronic. Eng.* 50 (2000) 357-368.

92. S.M. Sze, *Physics of Semiconductor Devices*, 2nd ed., John Wiley & Sons Inc., New York, 1981, p. 434.
93. S.J.Yun, K.-H. Lee, J. Skarp, H.-R. Kim, and K.-S. Nam, *J. Vac. Sci. Technol.* A. 15 (1997) 2993-2997.
94. E.P. Gusev, M. Gopel, E. Cartier, I.J.R. Baumvol, C. Krug, and M.A. Gribelyuk, *Appl. Phys. Lett.* 76 (2000) 176-178.
95. K. Kukli, K. Forsgren, J. Aarik, T. Uustare, A. Aidla, A. Niskanen, M. Ritala, M. Leskelä, and A. Hårsta, *J. Cryst. Growth* 231 (2001) 262-272.
96. K. Kukli, K. Forsgren, M. Ritala, M. Leskelä, J. Aarik, and A. Hårsta, *J. Electrochem. Soc.* 148 (2001) F227-F232.
97. H. Zhang and R. Solanki, *J. Electrochem. Soc.* 148 (2001) F63-F66.
98. O. Sneh, R.B. Clark-Phelps, A.R. Londergan, J. Winkler, and T.E. Seidel, *Thin Solid Films* 402 (2002) 248-261.
99. I. De, D. Johri, A. Srivastava, and C.M. Osburn, *Solid-State Electron.* 44 (2000) 1077-1080.
100. M. Ritala and M. Leskelä, *Handbook of Thin Film Materials*, Ed. H.S. Nalwa, Academic Press, San Diego 2001, Vol.1, p.103-113.
101. M. Ritala, M. Leskelä, J.-P. Dekker, C. Mutsaers, P.J. Soininen, and J. Skarp, *Chem. Vap. Deposition* 5 (1999) 7-9.
102. C.-S. Shin, D. Gall, P. Desjardins, A. Vailionis, H. Kim, I. Petrov, J.E. Greene, and M. Odén, *Appl. Phys. Lett.* 75 (1999) 3808-3810.
103. K. Hieber, *Thin Solid Films* 24 (1974) 157-164.
104. T. Takahashi, H. Itoh, and S. Ozeki, *J. Less-Common Met.* 52 (1977) 29-36.
105. X.C. Chen, G.G. Peterson, C. Goldberg, G. Nuesca, H.L. Frisch, A.E. Kaloyeros, B. Arkles, and J. Sullivan, *J. Mater. Res.* 14 (1999) 2043-2052.
106. X. Chen. H.L. Frisch, A.E. Kaloyeros, B. Arkles, and J. Sullivan, *J. Vac. Sci. Technol.* B 17 (1999) 182-185.
107. R. Fix, R.G. Gordon, and D.M. Hoffman, *Chem. Mater.* 5 (1993) 614-619.
108. C.-H. Han, K.-N. Cho, J.-E. Oh, S.-H. Paek, C.-S. Park, S.-I. Lee, M.Y. Lee, and J.G. Lee, *Jpn. J. Appl. Phys.* 37 (1998) 2646-2651.
109. K.-N. Cho, C.-H. Han, K.-B. Noh, J.-E. Oh, S.-H. Paek, C.-S. Park, S.-I. Lee, M.Y. Lee, and J.G. Lee, *Jpn. J. Appl. Phys.* 37 (1998) 6502-6505.
110. M.H. Tsai, S.C. Sun, H.T. Chiu, C.E. Tsai, and S.H. Chuang, *Appl. Phys. Lett.* 67 (1995) 1128-1130.

111. M.H. Tsai, S.C. Sun, C.P. Lee, H.T. Chiu, C.E. Tsai, S.H. Chuang, and S.C. Wu, *Thin Solid Films* 270 (1995) 531-536.
112. H.-T. Chiu and W.-P. Chang, *J. Mater. Sci. Lett.* 11 (1992) 96-98.
113. J.-M.M. Lehn, P. van der Heide, Y. Wang, S. Suh, and D.M. Hoffman, *J. Mater. Chem.* 14 (2004) 3239-3245.
114. C.H. Winter, K.C. Jayaratne, and J.W. Proscia, *Mat. Res. Soc. Symp. Proc.* 327 (1994) 103-108.
115. A.C. Newport, J.E. Bleau, C.J. Carmalt, I.P. Parkin, and S.A. O'Neill, *J. Mater. Chem.* 14 (2004) 3333-3336.
116. L. Hiltunen, M. Leskelä, M. Mäkelä, L. Niinistö, E. Nykänen, and P. Soininen, *Thin Solid Films* 166 (1988) 149-154.
117. M. Ritala, P. Kalsi, D. Riihelä, K. Kukli, M. Leskelä, and J. Jokinen, *Chem. Mater.* 11 (1999) 1712-1718.
118. H. Kim, A.J. Kellock, and S.M. Rossnagel, *J. Appl. Phys.* 92 (2002) 7080-7085.
119. H. Kim, C. Lavoie, M. Copel, V. Narayanan, D.-G. Park, and S.M. Rossnagel, *J. Appl. Phys.* 95 (2004) 5848-5855.
120. Y.Y. Wu, A. Kohn, and M. Eizenberg, *J. Appl. Phys.* 95 (2004) 6167-6174.
121. W.F.A. Besling, M.-L. Ignacimouttou, A. Humbert, M. Mellier, and J. Torres, *Microelectronic Eng.* 76 (2004) 60-69.
122. K.-I. Na, S.-J. Park, W.-C. Jeong, S.-H. Kim, S.-E. Boo, N.-J. Bae, and J.-H. Lee, *Mat. Res. Soc. Symp. Proc.* 766 (2003) E3.22.1-E3.22.6.
123. J.-S. Park, H.-S. Park, and S.-W. Kang, *J. Electrochem. Soc.* 149 (2002) C28-C32.
124. O. van der Straten, Y. Zhu, K. Dunn, E.T. Eisenbraun, and A.E. Kaloyeros, *J. Mater. Res.* 19 (2004) 447-453.
125. J.-S. Park, M.-J. Lee, C.-S. Lee, and S.-W. Kang, *Electrochem. Solid-State Lett.* 4 (2001) C17-C19.
126. O. van der Straten, Y. Zhu, J. Rullan, K. Topol, K. Dunn, and A. Kaloyeros, *Mat. Res. Soc. Symp. Proc.* 812 (2004) F3.13.1-F3.13.6.
127. D. Cheng and E.T. Eisenbraun, *Mat. Res. Soc. Symp. Proc.* 766 (2003) E10.4.1-E10.4.6.
128. H. Kim and S.M. Rossnagel, *49th International American Vacuum Society Conference*, Denver 2002.
129. J.-S. Min, H.-S. Park, and S.-W. Kang, *Appl. Phys. Lett.* 75 (1999) 1521-1523.

130. H. Kim and S.M. Rossnagel, *American Vacuum Society Topical Conference on Atomic Layer Deposition 2002*, Seoul (2002).
131. C.H. Peng, C.H. Hsieh, C.L. Huand, J.C. Lin, M.H. Tsai, M.W. Lin, C.L. Chang, W.S. Shue, and M.S. Liang, *IEDM Tech. Dig.* (2002) p. 603-606.
132. H. Chung, M. Chang, S. Chu, N. Kumar, K. Goto, N. Maity, S. Sankaranarayanan, H. Okamura, N. Ohtsuka, and S. Ogawa, *Proceedings of the IEEE 2003 International Symposium on Semiconductor Manufacturing Conference* (IEEE, San Jose, CA 2003) p. 454-456.
133. O. van der Straten, Y. Zhu, E. Eisenbraun, and A. Kaloyeros, *Mat. Res. Soc. Symp. Proc.* 716 (2002) B11.3.1-B11.3.6.
134. O. van der Straten, Y. Zhu, E. Eisenbraun, and A. Kaloyeros, *Proceedings of the IEEE International Interconnect Technology Conference* (IEEE, New York, N.Y 2002) p. 188-190.
135. K.-J. Choi and S.-G. Yoon, *Electrochem. Solid-State Lett.* 7 (2004) G47-G49.
136. C.S. Olsen, P.A. Kraus, K.Z. Ahmed, S. Kher, S. Hung, N. Krishna, J. Chen, L. Date, M. Burey, J. Campbell, C.-H. Lu, M. Deal, and Y. Nishi, *Mat. Res. Soc. Symp. Proc.* 811 (2004) D4.3.1-D4.3.5
137. Y.-S. Suh, G.P. Heuss, J.-H. Lee, and V. Misra, *IEEE Electron Dev. Lett.* 24 (2003) 439-441.
138. Y.-S. Suh, G. Heuss, and V. Misra, *J. Vac. Sci. Tehnol.* B 22 (2004) 175-179.
139. K. Baba, R. Hatada, K. Udoh, and K. Yasuda, *Nucl. Instrum. Methods Phys. Res.* B 127/128 (1997) 841-845.
140. A. Bendavid, P.J. Martin, T.J. Kinder, and E.W. Preston, *Surf. Coat. Technol.* 163-164 (2003) 347-352.
141. G. Oya and Y. Onodera, *J. Vac. Sci. Technol.* 7 (1970) S44-S47.
142. G. Oya and Y. Onodera, *Jpn. J. Appl. Phys.* 10 (1971) 1485-1486.
143. G. Oya and Y. Onodera, *J. Appl. Phys.* 45 (1974) 1389-1397.
144. G. Oya and Y. Onodera, *J. Appl. Phys.* 47 (1976) 2833-2840.
145. T. Takahashi, H. Itoh, and T. Yamaguchi, *J. Cryst. Growth* 46 (1979) 69-74.
146. G.M. Demyashev, V.R. Tregulov, and R.K. Chuzhko, *J. Cryst. Growth* 63 (1983) 135-144.
147. G.M. Demyashev, V.R. Tregulov, and A.A. Gavrich, *J. Cryst. Growth* 87 (1988) 33-40.

148. R.G. Gordon, X. Liu, R.N.R. Broomhall-Dillard, and Y. Shi, *Mat. Res. Soc. Symp. Proc.* 564 (1999) 335-340.
149. C.W. Wu, W.C. Gau, J.C. Hu, T.C. Chang, C.H. Chen, C.J. Chu, and L.J. Chen, *Surf. Coat. Technol.* 163-164 (2003) 214-219.
150. W.C. Gau, C.W. Wu, T.C. Chang, P.T. Liu, C.J. Chu, C.H. Chen, and L.J. Chen, *Thin Solid Films* 420-421 (2002) 548-552.
151. X. Liu, J.R. Babcock, M.A. Lane, J.A. Belot, A.W. Ott, M.V. Metz, C.R. Kannewurf, R.P.H. Chang, and T.J. Marks, *Chem. Vap. Deposition* 7 (2001) 25-28.
152. P.A. Bates, A.J. Nielson, and J.M. Waters, *Polyhedron* 4 (1985) 1391-1401.
153. V.P. Anitha, S. Major, D. Chandrashekharam, and M. Bhatnagar, *Surf. Coat. Technol.* 79 (1996) 50-54.
154. M.S. Mudholkar and L.T. Thompson, *J. Appl. Phys.* 77 (1995) 5138-5143.
155. R.M. Fix, R.G. Gordon, and D.M. Hoffman, *J. Am. Chem. Soc.* 112 (1990) 7833-7835.
156. R. Fix, R.G. Gordon, and D.M. Hoffman, *Thin Solid Films* 288 (1996) 116-119.
157. T. Nakajima and T. Shirasaki, *J. Electrochem. Soc.* 144 (1997) 2096-2100.
158. S.L. Roberson, D. Finello, and R.F. Davis, *Surf. Coat. Technol.* 102 (1998) 256-259.
159. S.L. Roberson, D. Finello, and R.F. Davis, *Thin Solid Films* 324 (1998) 30-36.
160. R.A. Waldo, *Microbeam Anal.* (1988) 310-314.
161. J. Jokinen, J. Keinonen, P. Tikkanen, A. Kuronen, T. Ahlgren, and K. Nordlund, *Nucl. Instrum. Methods Phys. Res.* B 119 (1996) 533-542.
162. J. Jokinen, P. Haussalo, J. Keinonen, M. Ritala, D. Riihelä, and M. Leskelä, *Thin Solid Films* 289 (1996) 159-165.
163. J.R. Hauser and K. Ahmed, *AIP Conference Proceedings* 449 (1998) (Conference on Characterization and Metrology for ULSI Technology) 235-239.
164. M.G. Simmonds and W.L. Gladfelter, *The Chemistry of Metal CVD*, Eds T.T. Kodas and M.J. Hampden-Smith, VCH, Weinheim 1994, p. 70.
165. M. Juppo, A. Rahtu, and M. Ritala, *Chem. Mater.* 14 (2002) 281-287
166. M. Eizenberg, K. Littau, S. Ghanayem, M. Liao, R. Mosely, and A.K. Sinha, *J. Vac. Sci. Technol.* A 13 (1995) 590-595.

167. M. Eizenberg, K. Littau, S. Ghanayem, A. Mak, Y. Maeda, M. Chang, and A.K. Sinha, *Appl. Phys. Lett.* 65 (1994) 2416-2418.
168. Q.Y. Zhang, X.X. Mei, D.Z. Yang, F.X. Chen, T.C. Ma, Y.M. Wang, and F.N. Teng, *Nucl. Instrum. Methods Phys. Res.* B 127/128 (1997) 664-668.
169. M. Juppo, P. Alén, M. Ritala, and M. Leskelä, *Chem. Vap. Deposition* 7 (2001) 211-217.
170. D. Riihelä, M. Ritala, R. Matero, M. Leskelä, J. Jokinen, and P. Haussalo, *Chem. Vap. Deposition* 2 (1996) 277-283.
171. *CRC Handbook of Chemistry and Physics*, 82nd ed., Ed. D.R. Lide, CRC Press LLC, 2001-2002, p. 9-65.
172. B. Hahn, M. Deufel, M. Meier, M.J. Kastner, R. Blumberg, and W. Geghardt, *J. Cryst. Growth* 170 (1997) 472-475.
173. G.B. Stringfellow, *Organometallic Vapor-Phase Epitaxy-Theory and Practise*, Academic Press Inc., San Diego, CA, 1989, p. 181.
174. M. Juppo, P. Alén, M. Ritala, T. Sajavaara, J. Keinonen, and M. Leskelä, *Electrochem. Solid-State Lett.* 5 (2002) C4-C6.
175. R.G. Gordon, D.M. Hoffman, and U. Riaz, *Chem. Mater.* 2 (1990) 480-482.
176. M. Boudreau, M. Boumerzoug, P. Mascher, and P.E. Jessop, *Appl. Phys. Lett.* 63 (1993) 3014-3016.
177. R.A. Levy, X. Lin, J.M. Grow, H.J. Boeglin, and R. Shalvoy, *J. Mater. Res.* 11 (1996) 1483-1488.
178. T. Aoki, T. Ogishima, A.M. Wróbel, Y. Nakanishi, and Y. Hatanaka, *Vacuum* 51 (1998) 747-750.
179. M.G. Boudreau, S.G. Wallace, G. Balcaitis, S. Murugkar, H.K. Haugen, and P. Mascher, *Appl. Opt.* 39 (2000) 1053-1058.
180. N. Terao, *J. Less-Common Met.* 23 (1971) 159-169.
181. M. Juppo, M. Vehkamäki, M. Ritala, and M. Leskelä, *J. Vac. Sci. Tech.* A 16 (1998) 2845-2850.
182. *Joint Committee on Powder Diffraction Standards*, File No. 25-1366.
183. *Joint Committee on Powder Diffraction Standards*, File No. 25-1367.
184. D. Vogler and P. Doe, *Solid State Technology* (January 2003) 35-40.
185. L. Peters, *Semiconductor International* (March 2003) 50-54.
186. H. Kim, *J. Vac. Sci. Technol.* B 21 (2003) 2231-2261.